Universidade do Minho
Escola de Engenharia

Ana Isabel de Araújo Coelho

A 3D computer assisted Orthopedic Surgery Planning approach based on planar radiography

outubro de 2015

Ana Isabel de Araújo Coelho **A 3D computer assisted Orthopedic Surgery Planning approach based on planar radiography**

UMinho | 2015

Universidade do Minho
Escola de Engenharia

Ana Isabel de Araújo Coelho

A 3D computer assisted Orthopedic Surgery Planning approach based on planar radiography

Dissertação de Mestrado
Mestrado Integrado em Engenharia Biomédica
Ramo de Informática Médica

Trabalho efetuado sob a orientação do
Professor Doutor Victor Manuel Rodrigues Alves
e do
Mestre João Pedro de Araújo Ribeiro

outubro de 2015

Declaração

Nome: Ana Isabel de Araújo Coelho

Endereço eletrónico: acoelho.tkd@gmail.com

Título da Dissertação: A 3D computer assisted Orthopedic Surgery Planning approach based on planar radiography

Orientador: Professor Doutor Victor Manuel Rodrigues Alves
Supervisor na Empresa: Mestre João Pedro de Araújo Ribeiro

Ano de conclusão: 2015

Designação do Mestrado: Mestrado Integrado em Engenharia Biomédica
Área de Especialização: Ramo de Informática Médica

Universidade do Minho, ___ / ___ / ___

Assinatura: _____

Ackowledgments

Firstly, I would like to express my sincere gratitude to Professor Victor Alves for the continuous support as well as for the autonomy and confidence deposited in me.

I would like to thank João Pedro, Jaime and Sara from PeekMed for all the suggestions, motivation, advices and support given throughout the development of this dissertation and without which its realization would be much harder.

I thank my friend Ramiro for the friendship, company, support and for the exchange of ideas during the development of this work.

Also, a special thank to my Taekwondo family for all the motivation given, for their interest on the state of development of this dissertation and for the relaxing moments provided and which greatly helped me.

I thank my parents and sister for the care, support and dedication.

Last but not the least, I would like to thank Tiago for the support, affection and motivation given always in the right moments.

Resumo

O principal objetivo deste trabalho consistiu em desenvolver um sistema capaz de realizar a reconstrução 3D de modelos ósseos a partir de imagens radiográficas. Este sistema pode posteriormente ser integrado num produto comercial que realiza o planeamento pré-operativo de cirurgias ortopédicas. O benefício de realizar esta reconstrução 3D a partir de radiografias está relacionado com o facto desta modalidade ter vantagens em relação às outras modalidades que fazem esta reconstrução diretamente, como as modalidades CT e MRI.

Para desenvolver este sistema foram usadas imagens radiográficas do fémur obtidas através de bases de dados online de imagens médicas. Também foi usado um modelo genérico do fémur disponível no repositório online BEL. Este modelo genérico completa a informação que está em falta nas imagens radiográficas. Foram desenvolvidos dois métodos, que realizam a reconstrução 3D através da deformação do modelo genérico sendo que num é feita a triangulação de pontos dos contornos e noutro não.

O primeiro método não foi bem sucedido, visto que o modelo final tinha uma espessura muito pequena, possivelmente devido ao facto do processo de triangulação não ter sido executado corretamente. Com o segundo método foi obtido um modelo 3D do fémur alinhado com as imagens radiográficas do paciente e com o mesmo tamanho do osso do paciente. No entanto, o modelo obtido carece ainda de alguma afinação de modo a coincidir na íntegra com a realidade. Para fazer isto é necessário melhorar o passo de deformação do modelo, para que este fique com a mesma forma do osso do paciente.

O segundo método é mais vantajoso porque não necessita dos parâmetros dos sistema de raios-X. No entanto, é necessário melhorar o passo de deformação deste método para que o modelo final coincida com a anatomia do paciente.

Abstract

The main goal of this work consisted in develop a system to perform the 3D reconstruction of bone models from radiographic images. This system can be then integrated with a commercial software that performs pre-operative planning of orthopedic surgeries. The benefit of performing this 3D reconstruction from planar radiography is that this modality has some advantages over other modalities that perform this reconstruction directly, like CT and MRI.

To develop the system it was used radiographic images of the femur obtained from medical image databases online. It was also used a generic model of the femur available in the online repository BEL. This generic model completes the information missing in the radiographic images. It was developed two methods to perform the 3D reconstruction through the deformation of the generic model, one uses triangulation of extracted edge points and the other don't.

The first method was not successful, the final model had very low thickness, possibly because the triangulation process was not performed correctly. With the second method it was obtained a 3D bone model of the femur aligned with the radiographic images of the patient and with the same size as the patient's bone. However, the obtained model still needs some adjustment to coincide fully with reality. To perform this is necessary to enhance the deformation step of the model so that it will have the same shape as the patient's bone.

The second method is more advantageous because it doesn't need the parameters of the x-ray imaging system. However, it's necessary to enhance the step deformation of this method so that the final model matches patient's anatomy.

Contents

List of Figures

Acronyms

2D Two Dimensional. 1, 3, 6, 8–14, 16, 19, 20, 23, 25, 29, 30, 32, 39, 43, 45–47, 52

3D Three Dimensional. xi, 1–4, 7, 9–16, 19–21, 23, 25, 26, 29–34, 37–39, 41, 43, 44, 47, 48, 52

AP Antero-Posterior. 19

BEL Biomechanics European Lab. 20

CAS Computer Assisted Surgery. 2, 11

CT Computed Tomography. 2, 3, 6–12, 15, 20

ITK Insight Segmentation and Registration Toolkit. 3, 38, 39, 42, 44, 45, 48, 49

LAT Lateral. 19

MRI Magnetic Resonance Imaging. 2, 3, 9, 10

PCL Point Cloud Library. 37

SPPM Simplified Personalised Parametric Model. 15, 16

VTK Visualization Toolkit. 3, 4

Chapter 1

Introduction

The three-dimensional reconstruction of patient specific bone structures is necessary in a variety of medical applications, more specifically in orthopedic applications.

Usually, the pre-operative planning of orthopedic surgeries is done with Two Dimensional (2D) images, like x-ray images, or sometimes the planning is not even performed. So, when the surgeon is going to perform the surgery, he is not well informed, because he doesn't know the exact anatomy of the patient, due to the use of only 2D images that don't give a view of the entire anatomy [1]. Also, he can't predict the possible complications that may occur during the surgery and also if no plan was done at all, he doesn't know the exact sizes of the prosthetic materials that may be needed to be implanted. All these conditions will increase the surgery time, which can be prejudicial to the patient because it increases the infection risk [2]. Also, the surgery accuracy will be lower, because the surgeon can use prosthetic materials that are not well suited for that particular patient and that will cause complications and sometimes it will be necessary to perform another surgery [3] .

So, Three Dimensional (3D) visualization of the bone structure, in the pre-operative planning, will be very helpful in many orthopedic surgeries, and enhance the accuracy of those surgeries [4]. Because with 3D bone models, the surgeon can visualize the entire anatomy of the bone, choose the most appropriate sizes of the prosthetic materials for that specific patient and predict some complications that may arise during the surgery.

One of the surgeries that can benefit from this technology is the arthroplasty, both knee and hip, because with the 3D patient-specific bone model it's possible to customize design of implant components. Therefore, it's achievable to overcome existing limitations of current generic designs. Another surgery whose accuracy could be enhaced with pre-operative 3D visualization is osteotomy.

This procedure is performed to straighten a bone that has healed crookedly following a fracture or to correct a congenital deformity. Thus the 3D visualization of the patient-specific bone model will help the surgeon plan the surgery, which will result in higher accuracy [3].

The 3D reconstruction of bone strutures can also be used in Computer Assisted Surgery (CAS) systems. In these type of systems it is necessary to register 3D patient-specific bone models to in vivo data real-time, so during the pre-operative planning is necessary to construct the 3D patient-specific bone model [5]. An example of a surgery that uses this type of systems is the fracture reduction procedure. This surgery recently have been performed with robotic devices and these use 3D models to reduce path planning and intra-operative tracking [3].

The 3D models of bone structures can also be used to personalize the treatment for pathologies such as scoliosis [6].

From what was described before, it's possible to affirm that a system to perform 3D reconstruction of bone structures will be helpful in the pre-operative planning of orthopedic surgeries.

1.1 Motivation

Usually 3D models are reconstructed from Computed Tomography (CT) or Magnetic Resonance Imaging (MRI) scans, however there are some disadvantages with these modalities. For example, CT induces high radiation doses to the patient, in fact, it's necessary to limit the number of scans to protect the patient [7]. Regarding MRI, this modality cannot be performed with metallic pieces, so when it's necessary to follow-up a patient with a metallic implant, it's not possible to do this with MRI scans [8].

Others disadvantages related with these modalities are their high costs, high acquisition time and also the acquisition of the scans in the supine position. This last disadvantage is an inconvenience for the clinical assessment of spinal deformities where it's necessary to acquire the scans in the natural standing position [6].

An alternative to these modalities is the planar radiography because this modality avoids exposure of the patient to high radiation, reduces the acquisition time and costs, and also allows the acquisition of the scan with the patient in the natural standing position [6].

So, planar radiography has advantages over CT and MRI and also is the most usually acquired exam in orthopedy. Therefore, it would be advantageous to construct a system that performs the 3D reconstruction of bone structures from planar radiography.

This work arises in the following of the work done by [9] and [10], where they constructed

a system to perform the orthopedic surgery planning based in 3D reconstruction from CT. In the present case, the work will focus in the 3D reconstruction of bone structures from 2D radiographic images.

In planar radiography modality it's possible to have one 2D planar radiographic image or two 2D orthogonal images, called posteroanterior and lateral images. The radiographic image is just a projection of the patient's body [11], where all the organs and bones are superimposed. So the surgeon has to mentally visualize the anatomy of interest [3]. Thus, the 3D reconstruction of radiographic images will be very helpful to the surgeon, because with this reconstruction he can actually visualize the bone and plan the surgery.

CT or MRI scans have several slices and that result in a lot of information about the anatomy of interest. However in radiographic images a lot of information is missing when only one or two orthogonal images are used [12], being hard to obtain a precise geometry of the bone structure with only this information.

Therefore, the problem of reconstructing a 3D model from radiographic images is a challenging assignment where it will be necessary to use additional knowledge of the bone structure in order to overcome the lack of information.

1.2 Goals

The main goal of this work is to construct a system to perform the 3D reconstruction of bone structures from planar radiography. Then, it's intended to integrate the developed system with Peekmed, a software package that allows performing the planning of orthopedic surgeries, this software will be described in the next chapter [13]. The surgeon can then plan the surgery with the 3D model of the patient's bone structure and also can have access to 3D templates of prosthetic materials, which will enhance the pre-operative planning of the surgery, leading to higher accuracy and reducing the surgery time.

To construct this system, the Insight Segmentation and Registration Toolkit (ITK) and Visualization Toolkit (VTK) libraries were used. ITK was developed by the Insight Software Consortium and is described as " an open-source, cross-platform system that provides developers with an extensive suite of software tools for image analysis. Developed through extreme programming methodologies, ITK employs leading-edge algorithms for registering and segmenting multidimensional data" [14]. This library is commonly used in the development of image registration and image segmentation programs. Normally, the images used for registration and segmentation are medical images. VTK

was developed by Kitware Inc., and "is an open-source, freely available software system for 3D computer graphics, image processing, and visualization" [15]. VTK has support for a large number of visualization algorithm and also has an extensive information visualization framework and has available a lot of 3D interaction widgets. In this work, this library was used for visualization of images and 3D models [15]. The programming language used was C++ and the IDE was Qt Creator.

1.3 Investigation Methodology

In the development of this work, the *action research* methodology was used. This methodology is described as "learning by doing" and constitutes a cycle. This cycle has five phases: first the problem is identified, second after considering all the possible solutions, a plan to implement a single solution is developed, third the solution is implemented, fourth it's evaluated the implemented solution and in the last phase it's decided if the results were satisfying, that is if the problem was solved, if not the process is repeated. The cycle is repeated until the problem is resolved [16].

1.4 Structure

This dissertation has the following structure: in the first chapter an introduction to the work is done, where the motivation, problem, goals and the investigation methodology used are presented; in the second chapter, some medical imaging systems and orthopedic surgery planning systems are described, also in this chapter is done a state of the art of the developed techniques to perform the 3D reconstruction from planar radiography; in the third chapter the materials and methods used in this work are referred and also the obtained results are presented; in the fourth chapter, the discussion of the results achieved is done and some conclusions and future work are referred.

Chapter 2

Medical Imaging and Surgery Planning

2.1 X-ray imaging system

The x-ray imaging system is composed by the x-ray source, the object/body and the x-ray detector. The object/body is between those two, so the x-rays will be directed to it [17].

In Figure 2.1 it's possible to observe a representation of a typical x-ray radiographic system [18].

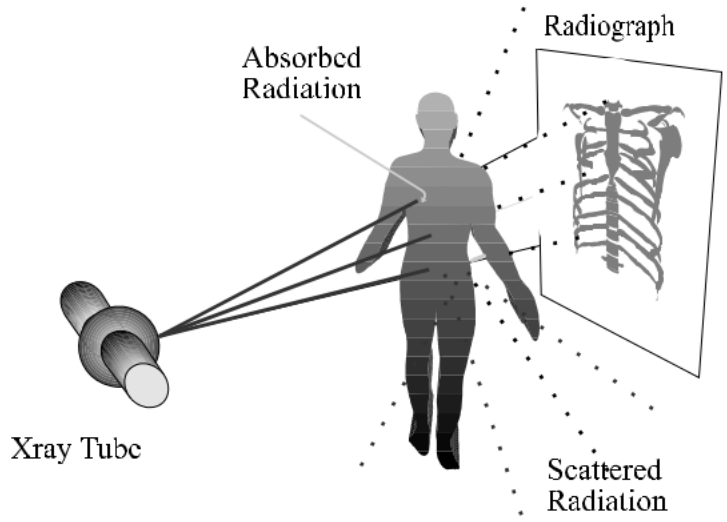

Figure 2.1: Representation of x-ray imaging system

When a beam of x-rays is directed at the human body, a fraction of photons will pass through without interaction, other fraction will be absorbed and others will be scattered. The relative proportions of transmission, absorption and scatter will change as the beam moves across the body.

These changes occur as the beam encounters more or less bone, soft tissue or blood [18].

So, the x-ray image records transmission of x-rays through the body and represents a 2D projection of the exposed anatomy [18].

In an ideal scenario, the contrast in an x-ray image would be produced only by the variation in the number of photons that pass through the body and reach the detector. These photons will form sharp-edge shadows. However some photons can be scattered by body tissue. Thus each point in the image can receive these additional photons that reach the detector from a wide range of positions in the body. They will cause the blurring of the sharp shadows [18].

The amount of radiation that is absorbed and scattered by a small region of tissue can be added together. This addition will correspond to the amount of radiation that is taken out of the direct transmitted beam. This amount represents the linear x-ray attenuation coefficient. This coefficient varies with tissue type and density and it's this variation that creates the contrast in x-ray images [18].

The regions with higher attenuation coefficient like bone will absorb more photons thus less photons will reach the detector and this regions will appear whiter in the image [19]. The regions with lower attenuation coefficient like soft tissue will transmit more photons thus more photons will reach the detector and these regions will appear darker in the image [19].

2.2 CT imaging system

A CT can be described as a "noninvasive medical examination or procedure that makes use of a specialized x-ray equipment to produce cross-sectional images of the body" [20]. These cross sectional images or slices are the result of multiple x-ray images taken from different angles and in these images it's possible to see bones, blood vessels and soft tissue [21]. The final result of a CT exam is called a CT scan and it's composed by all the slices taken during the exam.

A CT can be performed on every region of the body and for multiple purposes. It can be used to verify the existence of internal injuries in multiple types of trauma, to diagnose other injury or diseases, or to plan medical, surgical or radiation treatment [21].

In Figure 2.2 is illustrated the CT imaging system. This system is composed by a motorized table and the CT machine. The CT machine as an x-ray source and a set of x-ray detectors on the opposite side as it's demonstrated in Figure 2.2. The x-ray source produces a narrow, fan-shaped beam that will reach the detectors on the other side. While the patient is inside the opening the x-ray source and the detectors will rotate around the patient. During the rotation the beam of x-rays will pass through a section of the patient's body and produce a slice image. The motorized table will

move the patient through the CT machine. During the rotation, in axial CT, the table is stationary and after that the table will be moved in order to acquire the next slice. In helical CT, the table moves continuously during the rotation which will produce a helical or spiral scan. The CT machine can have a single row of detectors or multiple rows. The use of multiple rows allows to acquire a higher number of slices simultaneously, which will reduce the overall time of the exam. All the images taken in the multiple rotations are in the end processed by computer in order to produce a series of image slices [22].

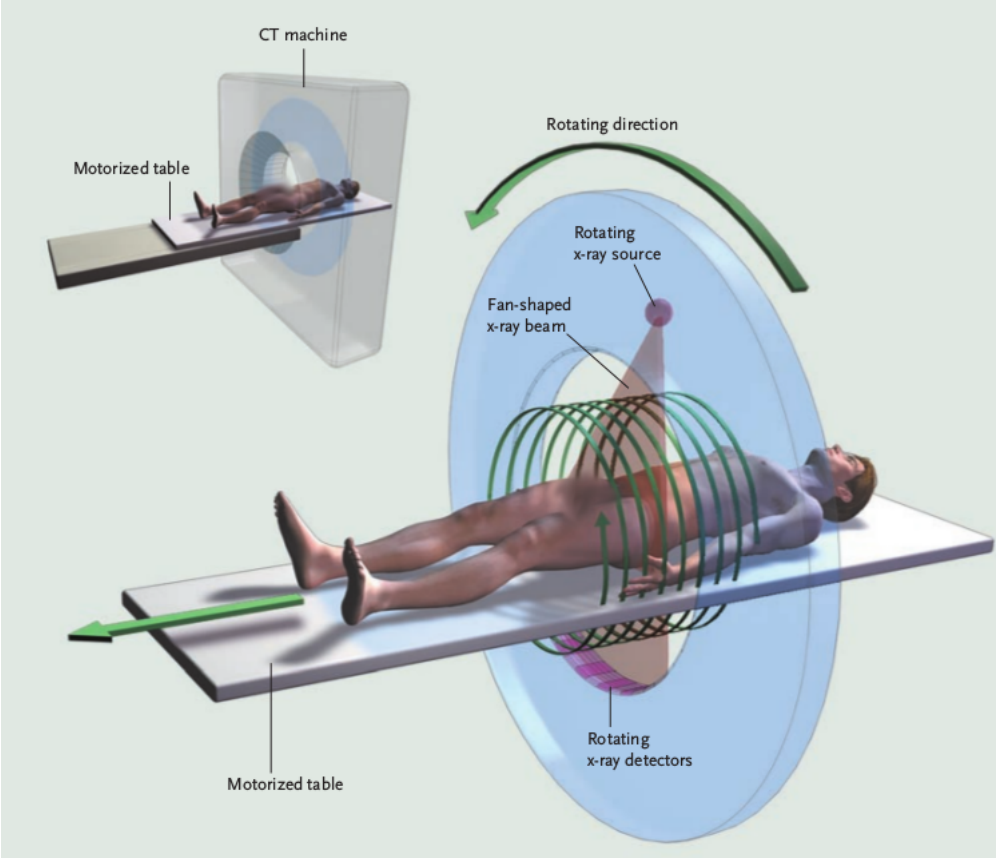

Figure 2.2: Representation of CT imaging system

The main advantage of this modality is that the slice images produced, resulting from multiple x-ray images of the patient's body taken from different angles, represent a volume, that is, a 3D view of the patient's anatomy being examined. So, with CT scans it's possible to recovery the 3D anatomy of the patient very easily.

However, this modality involves larger radiation doses in comparison with x-ray modality. Be-

cause in CT several x-ray images are taken, so the radiation involved in one single x-ray image is multiplied by the number of images taken, which will result in large amounts of radiation. And this can result in diseases, like cancer, for the patients.

2.3 Orthopedic Surgery planning

The preoperative planning of a surgery is a crucial step because it is in this stage that the surgeon will better understand the problem that he will face in the surgery. Thus, if the surgeon is well prepared for the surgery, the probability of surgery's success is higher than if the surgeon is not prepared. That is why preoperative planning systems are very important. Even more in the orthopedic area because in these type of surgeries sometimes it's necessary to place implants in the patient and if this task is not well succeeded, the patient will have postoperative complications and in some cases it is necessary to perform another surgery. A preoperative planning system is a system that helps the surgeon perform the planning of a surgery by providing measurement tools, prosthetic implant templates and other tools. With this, the surgeon can perform the necessary measurements, choose the most appropriate implant for the patient, predict complications and so he will be more prepared for the surgery. In fact, preoperative planning can help enhance surgery accuracy, efficiency and reproducibility. It also can prevent use of undersized and oversized implants and can allow the better visualization and manipulation of the lesion [23].

2.3.1 2D Preoperative Planning

In the case of orthopedic surgeries, until the appearance of digital radiographic images, the preoperative planning was done with the 2D radiographic images, light boxes, tracing paper and transparent bone and prostheses templates [1]. In this situation, the preoperative planning is done by overlaying the transparent prostheses templates on the radiographic images in order to determine the most appropriate prosthesis [24].

The appearance of digital radiographic equipment have improved the preoperative planning of orthopedic surgeries. This lead to the appearance of digital planning software. However, the software developed at the moment work only with 2D radiographic images and it's still not possible to manipulate the fracture or to select the prosthesis [1].

The main features of these software are the possibility to perform measurements, to select an implant from a database, manipulate it and place it on the digital radiographic image, to simulate

surgeries and inspect their results and also to create pre-surgical reports that include patient images, implant information, measurements taken and comments [25–28].

Some examples of this type of software that are in the market are TraumaCad [25], OrthoView [26], Merge OrthoCase [27] and IMPAX [28].

Some of these software perform automatic measurements accordingly to the surgery that will be performed and suggest automatically an implant size and placement based on the radiographic image. It's the case of Merge OrthoCase [27].

One of the advantages of these digital planning software is the reduction of the costs of image production and storage. The use of digital radiographic images instead of the traditional plain film radiographs eliminated the need of printing and storing them. With these software all the files related to the preoperative planning of the surgery, including the radiographic images, are recorded in a digital environment [23].

Another advantage is the scaling of the image to the true size of the patient's anatomy. Thus, the surgeon doesn't need to work with standard magnification factors for implant templates [28].

One more advantage is the selection of implants from a database. This database is constituted of templates from a wide variety of international manufacturers. This allow the surgeon to select the most appropriate implant for the patient's anatomy which will save surgery time and avoid possible complications that may occur due to inappropriate implants [3]. Some software also recommend positions and templates sizes which makes easier the final adjustments.

The preoperative planning of orthopedic surgeries relies only on 2D radiographic images, because CT or MRI modalities that allows direct 3D reconstruction are only available for more complex surgeries. This is due to their lower availability, higher radiation exposure and costs [1].

The planning of a procedure with only 2D images is complicated and can lead to errors that can make necessary to perform another surgery or can cause biomechanical defects [1]. The major problem of planning a surgery with only 2D images is the lack of spatial information along the view direction which will lead to visual ambiguities [24]. This makes necessary for the surgeon to mentally visualize the anatomy of interest, which requires more time in the surgery planning and also requires more knowledge and experience. Also, the use of 2D images could result in errors in the selection of the best implant, which may increase the surgery time in order to adapt the implant to the patient's anatomy or could lead to errors that can cause defects to the patient [3].

2.3.2 3D Preoperative Planning with CT scans

The emergence of more complex surgeries led to the need for better visualization and manipulation of the anatomy of interest, both in the preoperative planning and during the surgery [29]. The 3D reconstruction of the anatomy of interest appeared because of this necessity. The existence of direct 3D imaging modalities such as CT or MRI helped in the development of this technology.

These software use the 3D bone model reconstructed from CT or MRI scans to perform measurements both in 2D and 3D, to design patient-specific implants and also simulate surgeries and predict their results. The main differences between these type of software and the software described before are the use of 3D bone models instead of 2D images and the possibility to design the implant accordingly to the patient anatomy instead of choosing one from a database [13, 25, 30].

Some examples of this type of software that are in the market are PeekMed [13], TraumaCad [25] and Mimics [30].

In the case of Mimics, this software has a X-ray Module that allows to combine the patient's radiographic images with his 3D bone model reconstructed from CT or MRI scans. So, it's possible to perform a 3D analysis with 2D radiographic images. This is done thanks to the manual contour-based or bead-based 2D/3D registration [30].

PeekMed is a 3D preoperative planning software for orthopedic surgery that provides the 3D planning of surgeries, simulation of fracture reduction, prosthetic materials in 3D and allows performing measurements. The main advantages of this particular software over the others existing is that it provides 3D templates of prosthetic materials, 3D models segmentation for trauma reduce and also the possibility to export to 3D printer. So, with this software it's possible to plan the surgery with both the 3D model of patient's specific bone and the 3D models of prosthetic materials. Thus, the surgeon can choose, in the preoperative stage, the most appropriate materials to use in the surgery which will lead to higher surgery accuracy [13].

With 3D models of the patient's specific bone structure, the surgeon doesn't need to mentally visualize the anatomy of interest [1]. These type of software also allow the surgeons to simulate the surgical procedure that will aid in predicting the problems that can arise during the procedure and prepare a plan to overcome these problems [31]. This better preparation of the surgery will result in a reduction of the surgery's duration which will be beneficial for both the patient and the surgeon. Because the surgeon will be more prepared to execute the surgery and consequently the patient will be under anesthesia for less time [2].

Also, 3D bone models will help define the implant requirements when the procedure involves

placement of an implant. The customization of the implants will lead to higher surgery accuracy and this is done much easier and efficiently with 3D bone models than with 2D images. With 3D bone models it's possible to create customized implants for those patients that have bone sizes outside the normal range. In this case, it's necessary to customize the implant because otherwise the implant won't fit properly and that can cause severe consequences to the patient [1]. Also, the 3D bone models will allow the surgeon to manipulate the fracture and better understand it. All these aspects will enhance the accuracy of the alignment and positioning of the implant and so improve the surgery's accuracy [3].

The main disadvantage of the preoperative planning software with 3D reconstruction from CT scans is the fact that this modality is only used in complex surgeries. This restraining is due to the lower availability of this modality, increased radiation exposure and higher costs [1]. So, these software can only be used when CT scans are available which is a very limited number of cases.

2.3.3 Computer Assisted Surgery with 3D models

3D bone models created in the preoperative planning can also be used during the surgery. CAS allow the visualization of these models and its registration with the images obtained intraoperatively. Next, there's an example of a procedure where the implementation of CAS will be very helpful.

Some orthopedic surgeries such as fracture reduction, pedicle screw insertion, total hip replacement and osteotomies, use fluoroscopic images intraoperatively. These images are used to determine the position of anatomy, surgical tools and implants relative to one another. They are also used to monitor the advance of guide wires, drills, and reamers, and to make corrections as necessary. However, this modality has some important limitations. Fluoroscopic images are static and 2D which requires the surgeon to mentally visualize the anatomy of interest and maintain hand-eye coordination while performing the surgery. Also, the images are static and the field of view is narrow, so the fluoroscope will be used more frequently, leading to a high radiation exposure to the surgeon. Another limitation is related to the geometric distortion that is present in the images of this modality, which makes it inappropriate to perform quantitative measurements and to perform accurate navigation. [32]

CAS can help to overcome those limitations. In these type of systems, 3D bone models, created during the preoperative planning, can be registered with the fluoroscopic images obtained intraoperatively and so the surgeon can observe the anatomy and instruments' positions in real time. This can reduce the surgeon's exposure to radiation, reduce surgical complications associated with align-

ment and positioning errors, reduce the surgery time and enhance preoperative planning, i.e., better visualization of the fracture and selection of the more appropriated implant. [32]

One example of the existing software of this type is Stryker [33].

These type of systems have the same disadvantage that the planning software described before, the use of CT scans for the 3D reconstruction.

2.3.4 3D Preoperative Planning with x-ray images

As mentioned before, a preoperative planning software with 3D models has more advantages for orthopedic surgery planning than the software that makes use of the 2D images. However, the existing software with 3D models perform the 3D reconstruction through CT scans and this modality it's only used in complex cases because of the disadvantages inherent to that modality.

Since the studies available in orthopedic surgery planning are often radiographic images, a software for preoperative planning that performs the 3D reconstruction through radiographic images will have many advantages. Also this modality has advantages over CT, namely, avoids exposure of the patient to high radiation and reduces the acquisition time and costs.

In the next section will be described the existing methods to perform 3D reconstruction from radiographic images.

2.4 3D reconstruction from x-ray images

The methods for 3D reconstruction of bone structures from 2D planar radiographic images can be divided in two types: the methods based only in the radiographic images and some a priori knowledge about topology and geometry of bone [34] and the methods based both in the radiographic images and in a template model of the bone structure that will be reconstructed [12].

2.4.1 Reconstruction without a template model

In Figure 2.3 is present the schematic overview for this reconstruction method. All the steps of the method will be described here.

In the first type of reconstruction it's necessary to obtain calibration points that will be used as parameters to the reconstruction algorithms. These points can be obtained either by manual identification of anatomical landmarks, with a calibration object or with both methods. In the case

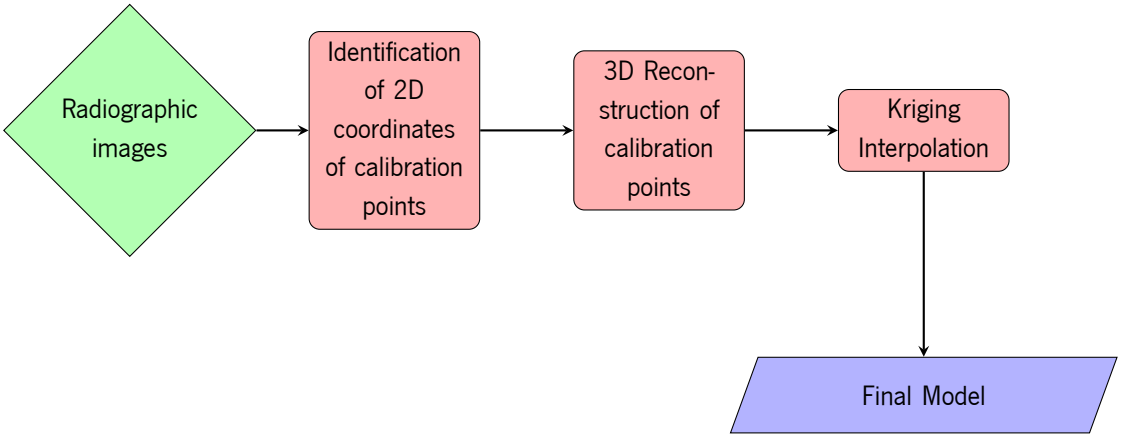

Figure 2.3: Flow Chart of reconstruction method without a template model

of the manual identification this task needs to be performed by an health care professional and can be very time consuming [6]. Regarding the calibration object, this object it's normally an acrylic plate with radio-opaque markers, usually steel balls, and it's used during the acquisition of the radiographic images [35]. The object is positioned so that the markers will be in specific locations, corresponding to anatomical landmarks [36].

After obtaining the calibration points it's possible to compute its 3D coordinates that will be used as parameters for the 3D reconstruction.

The points present in the two radiographic images are called stereo corresponding points and its 3D coordinates can be obtained using the DLT algorithm. This algorithm needs the 2D and 3D coordinates of some points to compute the DLT parameters. These parameters express the relationship between the 3D coordinates of the real point and the coordinates of its projection point on the plane image. Once determined the parameters, they will be used with the 2D coordinates of the point being reconstructed to determine the 3D coordinates of the stereo corresponding points. [37]

The points present in only one radiographic image are called non-stereo corresponding points and its 3D coordinates are obtained with the NSCP algorithm. In this algorithm it's assumed that any non-stereo corresponding point belongs to line joining its projection on the film and the X-ray source, which gives an estimation of the 3D position of the point. Then, a priori knowledge about the bone structure is used as topological and geometrical constraints to optimize this estimation. [34]

After reconstructing the 3D coordinates of the calibration points, the kriging algorithm is used to obtain the detailed model of the patient specific bone structure. This algorithm uses the reconstructed points and some a priori knowledge and interpolates this data. The interpolation is done

through deformation of a generic object. Then, the object resulting from interpolation will be the 3D model of patient specific bone structure. [34]

2.4.2 Reconstruction with a template model

In the second type of reconstruction, with a priori knowledge (template model) it's possible to complete the information that is missing in the radiographic images. The patient specific bone structure will result from the deformation of the template model [12].

In Figure 2.4 it's possible to observe the diagram describing the workflow for this method. All the steps comprising in this method will be explained next.

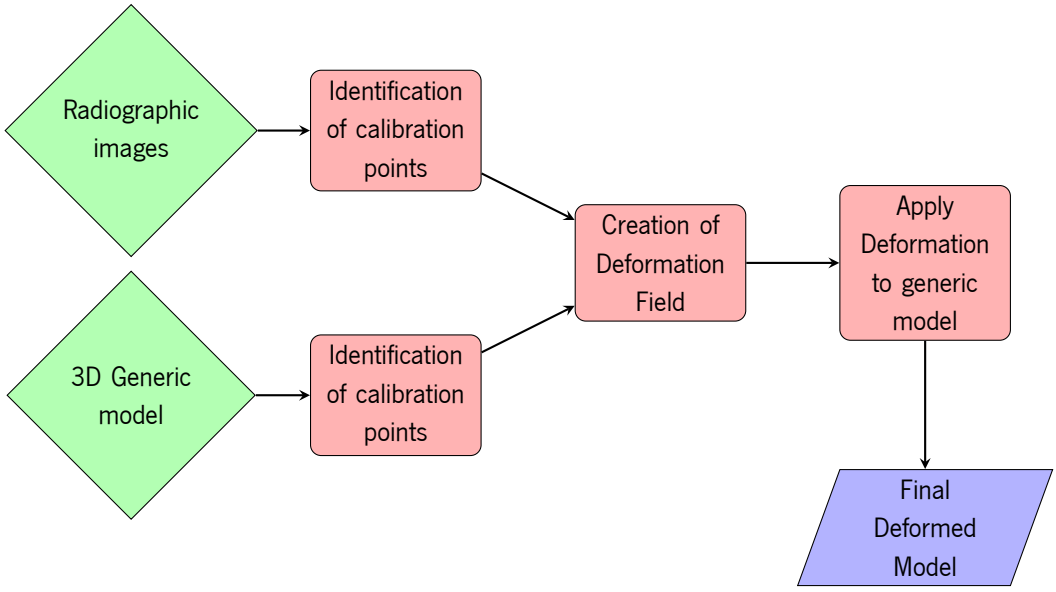

Figure 2.4: Flow Chart of reconstruction method with a template model

The template model of the bone structure is constructed with CT data of a population. Usually, is generated a statistical model, using PCA, that represents the different components of shape variation from the population [8]. The statistical model can also be created from a set of descriptors that are defined according to the anatomical landmarks identifiable in the radiographic images. This set of descriptors will be the input of the statistical model and are called the main descriptors. Then, a full set of descriptive parameters can be obtained through statistical inferences of the main descriptors. The result is the Simplified Personalised Parametric Model (SPPM) [38]. Another method to create a template model is by constructing a database of 3D models reconstructed from CT data. Then, all

these models as well as the radiographic images of the patient are scaled to a standard size in order to be compared. After the comparison, the most similar model is selected and scaled back to the original size of the patient's bone structure [39]. A simplest method is to obtain the template model through the 3D reconstruction of a CT scan from a healthy subject of normal height and weight [40].

In this type of reconstruction the definition of calibration points is also needed. In most cases this task is performed manually with a user identifying the points as in the first type described above. Only a few cases use a semi-automatic method to identify these points and they do it using a priori knowledge of the bone structure and advanced pattern recognition, mathematical, and geometrical techniques [5]. Other methods to perform this task include machine learning techniques [41]. This points could then be used to help in the extraction of the bone contours in the radiographic images [42], in the generation of the statistical model [43], to compute the matching error of reconstructed model [44] or to act as handles for the deformation [38].

An alternative to the definition of calibration points is the extraction of the bone contours from the radiographic images. First, it's applied the Gaussian filter to remove image noise and strength the image contrast of boundary region [44]. Then it's used the Canny Edge operator to define the sharp edges. The last step consists in applying the edge linking technique to create a continuous bone outline [39]. However, some deformation techniques require calibration points and thus the bone contours are not useful in these cases.

Once the template model is created it's possible to fit it to the patient specific bone structure. This is called the deformation step. One way to perform this, is using the descriptive parameters estimated from the statistical model and the anatomical landmarks to obtain a set of handles. Then, this handles will be used to deform a generic 3D model towards the SPPM, through an as rigid as possible MLS deformation. The model generated with this deformation can be refined by performing a local deformation with another set of handles and using the kriging interpolation. [38]

The step of deformation can also be performed using rigid transformations. For example, [45] created a geometrical model that fits the radiographic images using spheres, cylinder and other elements. Then, it's calculated an initial rigid transformation and a parameter set to adjust the statistical model to the geometrical model. After this, a 2D/3D non rigid registration is executed to adjust the extracted bone contours of radiographic images to the statistical model. From this last step will result an updated instance of the statistical model and a new rigid transformation. This will be repeated until the procedure converges or a limited number of times.

Another approach to deform the template model is the FFD technique. Briefly, this method consists in embed the model in a hull object that is deformable. Then, instead of deforming the

model directly, the hull is deformed, and consequently the model inside is also deformed. The hull can be called control volume/lattice and is characterized by control points that regulate the deformation [46]. The deformation can be defined as an optimization problem where the optimum combination of deformation parameters is searched. The purpose of this optimization is to minimize the differences between the radiographic images and the model [47].

All methods of reconstruction described in this section have some problems identified. For example, in the first method of reconstruction and in some cases of the second method is necessary to define calibration points. Usually, this is done through the manual identification of anatomical landmarks by a specialized user. This task is particularly time consuming, tedious and susceptible to error [6].

Also, in some cases of the first method, the definition of calibration points is done with a calibration object. This object is used during the acquisition of the radiographic images. This may constitute a problem because this object can not be always available. Also it has a different configuration for each bone structure, so there is a necessity in always changing its arrangement.

A problem identified in the second method regarding the statistical models is the need of extensive databases to construct them [12]. And in case of generic models, the use of this type of models increase the reconstruction time [36].

Chapter 3

Materials and Methods

In this chapter, first will be described the materials used in the development of this work. Then, the implemented method to perform the 3D reconstruction of bone models from radiographic images will be characterized. This description is divided in the various steps that constitute the method.

3.1 Data

3.1.1 X-ray Images

In this work, Antero-Posterior (AP) and Lateral (LAT) x-ray images of the femur were used.

X-ray images are the result of the transformations that a x-ray beam suffers when passing through the patient's body. A x-ray tube will produce the x-ray beam and this will pass through the body. On the other side of the body, a x-ray detector will receive the resulting x-rays and this will result in the final x-ray image. When passing through the body some photons of the x-ray beam will be absorbed, some scattered and the other will be transmitted. The x-ray image represents these transformations that the photons can experience when passing through the body. In these type of images, the whiter regions represents the regions where there is greater absorption of radiation, like the bone and the darker are the regions where are more photons transmitted and this occurs in the soft tissue. These images are 2D and all the organs and bones are superimposed [48].

In Figure 3.1 it's possible to observe the AP x-ray image of the femur that was used in this work. This image was downloaded from an online medical database.

Figure 3.1: AP x-ray image of the femur

3.1.2 3D bone model

A 3D generic bone model of the femur was obtained from the Biomechanics European Lab (BEL) Repository available in the BiomedTown website [49].

This model was constructed from CT scans of frozen cadaver and can be visualized in Figure 3.2.

A CT scan is a series of cross-sectional images of the body. These cross-sectional images are usually called slices. These slices are the result of multiple x-ray images taken from different angles as it was explained in the previous chapter. The great advantage of CT is that it allows the 3D reconstruction of the anatomy. In conventional x-ray images, all the planes are superimposed in a single 2D image, however in CT we have multiple x-ray images, that are the slices, and with those it's possible to construct a volume. This is done by stacking the slices one on top of the other.

Figure 3.2: 3D Generic bone model of the femur

Originally, the slices are in the axial plane, so by stacking the slices, an axial volume is obtained. However, there are techniques that allow the reconstruction of volumes in different planes. This technique is called MPR and first the axial volume is reconstructed and then slices are cut through the volume in different planes. With this technique it's possible to obtain volumes in axial, coronal and sagittal planes [50].

3.2 Reconstruction method with triangulation of anatomical landmarks

The first method implemented in this work to perform 3D reconstruction of bone models from radiographic images makes use of a generic bone model. This generic model will complete the information missing in the orthogonal radiographic images.

Figure 3.3 it's a schematic presentation of the workflow of this method. This method will be explained in detail in the next subsections.

In order to obtain the 3D patient's specific bone model it's necessary to deform the generic

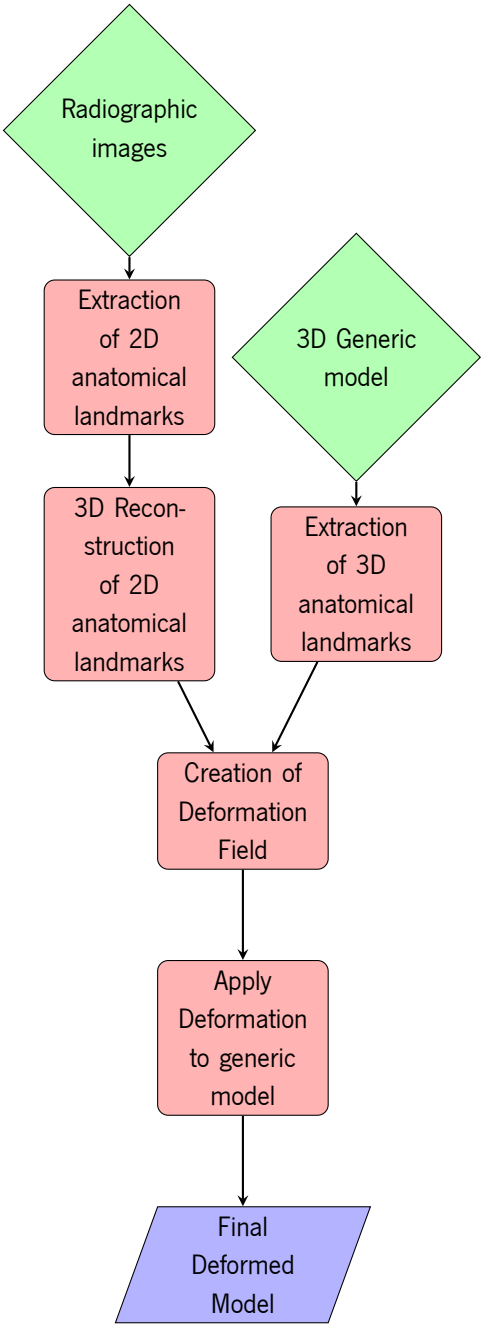

Figure 3.3: Flow Chart of reconstruction method with triangulation of anatomical landmarks

model. And to do this, it's necessary to know the deformation that needs to be applied. This deformation is known through the registration of the generic model with the original radiographic images. So, according to this, a 3D registration of landmarks of the model and the original radiographic

images was performed in order to obtain the deformation necessary to employ in the generic model. It was used a non-rigid registration based on a set of corresponding anatomical landmarks, in order to deform the model so that it will have the same shape as the bone present in the radiographic images.

This type of registration can be divided in three main steps: 1) extraction of landmarks in the different datasets; 2) establishing the correspondences between the landmarks; and 3) computing the transformation between the datasets using the information from 1) and 2) [51].

The first attempt was to perform a 2D/2D registration between the original radiographic images and the generic model's radiographic projections. First, the anatomical landmarks were extracted manually from the radiographic images and the model's projection. Then, the transformation between the two point sets was computed using a thin-plate splines interpolation. However this method resulted in a 2D deformation field and so it was only possible to apply a 2D deformation on the model. But it was intended to deform the model as a whole so it was necessary a 3D deformation field.

To obtain a 3D deformation field was necessary to perform a 3D/3D registration instead of a 2D/2D registration. In order to perform this type of registration, it was introduced a step before the registration of landmarks. This step was the 3D reconstruction of some points of the original radiographic images. With these 3D points it's possible to perform a 3D/3D registration and thus obtain a 3D deformation field. The process of reconstruct 3D points from 2D points on images is called triangulation and will be described later.

The last step of the reconstruction consisted in the deformation of the generic model. This step consists in apply the deformation field generated before to the generic model. The resulting model from this step will be the 3D patient's specific bone model.

3.2.1 Extraction of anatomical landmarks/contours

Firstly the extraction of anatomical landmarks was performed manually with the extraction of 2D points in the radiographic images and 3D points in the generic model. But, the results were very poor so instead of using anatomical landmarks it was used the edge points of the bone contours. This was performed using a Canny Edge algorithm to extract the 2D edge points in the radiographic images and the 3D edge points in the generic model. It was used the Canny Edge Algorithm provided by ITK library. This algorithm was developed by John Canny in 1986 and can be divided in five main steps [52]. These steps are detailed in Figure 3.4.

The first step is done in order to remove the noise present in the image. Because the edge

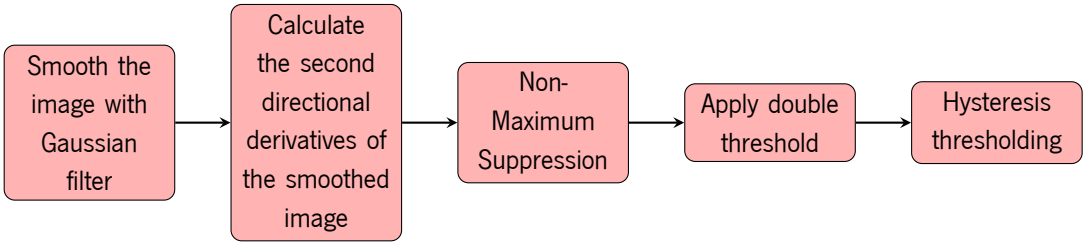

Figure 3.4: Flow Chart of Canny Edge algorithm

detection is easily affected by noise, so to prevent false detection, the noise is removed from image [52].

In the second step the edge gradient and direction are determined. However, the edges extracted in this step are quite blurred. So, the third step is used to "thin" the edges. The blurring of the edges occur because there's more then one accurate response to the edge. But, there should only exist one, so the non-maximum suppression is used to solve this problem. This method will suppress all the gradient values to 0 except the local maximal, which indicates location with the sharpest change of intensity value [52].

The fourth step corresponds to application of a double threshold. This is done because after the third step there are still some false detected edges due to noise and color variation. So, two threshold values are set to classify the edge pixels. If the edge pixel's gradient value is higher than the high threshold value, it is marked as strong edge pixel. If the edge pixel's gradient value is smaller than the high threshold value and larger than the low threshold value, it is marked as weak edge pixel. If the pixel value is smaller than the low threshold value, it is marked as a non edge pixel and will be suppressed [52].

The last step is used to determine the origin of the weak edge pixels, since this type of pixels can be derived from true edges or from noise. So, it's necessary to determine where these pixels came from, because if they are derived from noise they should be removed. This determination is done using the observation that the weak edge pixels that derive from true edge pixels will be connected to the strong edge pixel. So, the weak edge pixels are compared with its neighbours and if at least one of the neighbours is a strong edge pixel, that weak edge pixel is preserved [52].

As described here, the Canny Edge algorithm has some parameters that can be adjusted in order to obtain the best results for each images. These parameters are the upper and lower thresholds and also the variance. In this case, in order to detect the edge points on the radiographic images, it was used the following parameters:

- $variance = 2;$
- $upperThreshold = 7;$
- $lowerThreshold = 0;$

Because it was not possible to obtain both the frontal and lateral radiographic images for the femur, it was used the radiographic model projections in order to simulate the two orthogonal radiographic images. The process of creating these images will be explained later. In Figure 3.5 it's possible to observe the detected edge points on the model's radiographic projections. Figure 3.5a represents the detected edge points on the frontal radiographic projection and Figure 3.5b on the lateral projection. In the frontal projection, 1194 points were detected and 1133 points in the lateral projection.

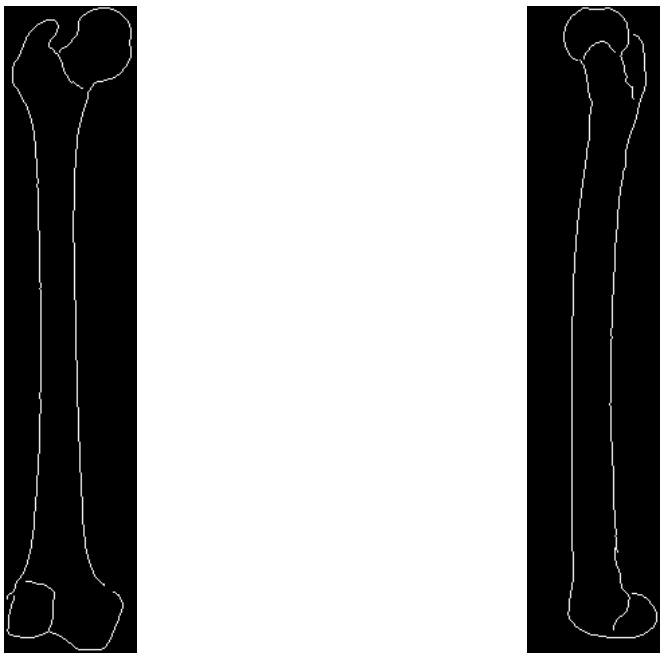

(a) Frontal edge points (b) Lateral edge points

Figure 3.5: Detected edge points on the model's radiographic projections

After this extraction, the 2D edge points of radiographic images were reconstructed to 3D with the technique described in the next section.

3.2.2 3D Reconstruction of edge contours

The 3D reconstruction of the 2D coordinates of edge contours, obtained in the previous step, was performed using the triangulation technique. This technique was performed based mostly on the work developed by Hartley and Zisserman [53]. Some concepts will be first described in order to better understand this technique and then the technique itself will be explained.

Epipolar Geometry

The epipolar geometry corresponds to the intrinsic projective geometry between two views. This is basically the geometry of the intersection of the image planes with the family of planes having the baseline as axis. The baseline corresponds to the line joining the camera centres [53].

This geometry is usually described for the problem of finding corresponding points in stereo matching. In this problem, supposing a point X in 3D space is imaged in two views and knowing the point x that corresponds to point X imaged in the first view, the objective is to find x' that is the point X imaged in the second view [53].

The image points x and x', space point X and camera centres belong to the same plane. Thus, they are coplanar and this plane can be called π. In Figure 3.6a, it's possible to observe this relation and it's also possible to observe that the rays back-projected from x and x' intersect at X [53]. These rays are also coplanar and belong to the same plane π. This last property is the most useful for the searching correspondence problem [53].

So, knowing only x and using the epipolar geometry it's possible to constrain the searching space for the corresponding point x'. The baseline and the ray defined by x will determine the plane π and as said before the ray defined by x' will also belong to π. So, it's possible to say that x' lies on the line of intersection of π with the second image plane. This line l' corresponds to the image in the second view of the ray defined by x and it's called epipolar line of x. Thus, with these relations, the search for the corresponding point x' is constrained to the line l' and not to the entire image plane. The geometry described here can be observed in Figure 3.6b [53].

In Figure 3.7 it's possible to observe the geometric entities associated with epipolar geometry. These entities are the following [53]:

- Epipole that is the point of intersection of the baseline with the image plane. It's also possible to describe this entity as the image in one view of the camera centre of the other view

- Epipolar plane that is any plane containing the baseline. This plane intersects the image

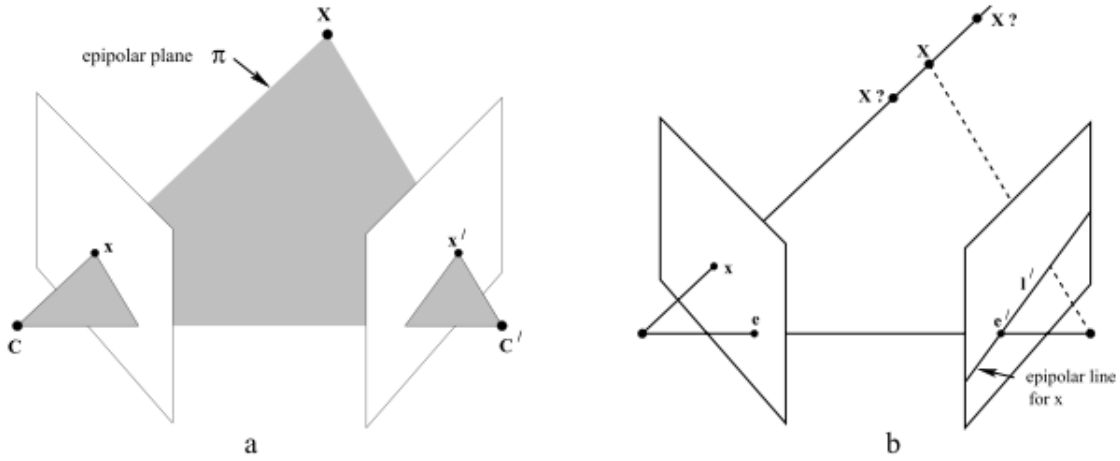

Figure 3.6: **Epipolar geometry.** (a) C and C' are the camera centres, X a 3D space point, x and x' its corresponding image points. All these points lie in the same plane π. (b) The baseline and the ray back-projected from x determine the plane π and this ray is imaged in the second view as a line l'. The 3D point X must lie on this ray, so x' must lie on line l'.

planes in corresponding epipolar lines l and l'.

- Epipolar line that is the intersection of an epipolar plane with the image plane. All epipolar lines intersect at the epipole.

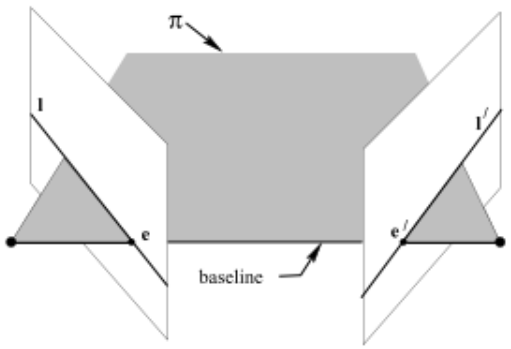

Figure 3.7: **Geometric entities of epipolar geometry.** e and e' are the epipoles, π is an epipolar plane and l and l' are the epipolar lines.

Fundamental Matrix

The epipolar geometry described before can be represented in a matrix, that is the fundamental matrix.

As it was exposed in the previous section, for each point x in one image, there is a corresponding epipolar line l' in the other image. And the corresponding point x' in the second image must lie on this line l'. So, it's possible to say that there is a map $x \mapsto l'$ from a point in one image to its corresponding epipolar line in the other image. This mapping is represented by the fundamental matrix.

This matrix satisfies the condition that for any pair of corresponding points (x, x') in the two images $x'^T F x = 0$. The importance of this condition is that with this it's possible to determine the fundamental matrix without knowing the camera matrices. To compute fundamental matrix it's only necessary to know image correspondences.

The most important properties of the fundamental matrix are the following:

- **Tranpose:** If F is the fundamental matrix of the pair of camera (P, P'), then F^T is the fundamental matrix of the pair in the opposite order (P', P)

- **Epipolar lines:** The epipolar line l' for any point x in the first image is $l' = Fx$. And the epipolar line l corresponding to point x' in the second image is $l = F^T x'$

- **Epipole:** For any point x the epipolar line $l' = Fx$ contains the epipole e'. So, e' satisfies $e'^T(Fx) = 0 = (e'^T F)x = 0$ for all x. Thus, $F^T e' = 0$ and $Fe = 0$

To perform the computation of fundamental matrix from point correspondences, the function findFundamentalMat of OpenCV library was used. This function uses the relation $x'^T F x = 0$ to compute the fundamental matrix. It also allows to choose the method used to compute the fundamental matrix. The methods available are 7-point algorithm, 8-point algorithm, RANSAC and LMedS. The 7-point algorithm requires an exact number of 7 point correspondences to find the fundamental matrix, the other methods require a minimum of 8 point correspondences. RANSAC and LMedS algorithms are used to get more robust results. The parameters of the function findFundamentalMat are the array of N points from the first image, the array of points from the second image with the same size of the first array and the method to compute the fundamental matrix. In this work, it was used the 8-point algorithm.

Camera matrices computation from Fundamental Matrix

The fundamental matrix computed before can be used to determine the camera matrices of the two views.

The relationships $l' = Fx$ and $x'^T F = 0$ are projective relationships. This happens because they depend only on projective coordinates in the image and not on Euclidean measurements, for example. So, this image relationships are projectively invariant, which means that under a projective transformation of the image coordinates $\widehat{x} = Hx$, $\widehat{x'} = H'x'$, there is a corresponding map $\widehat{l'} = \widehat{F}\widehat{x}$ with $\widehat{F} = H'^{-T} F H^{-1}$ the corresponding fundamental matrix [53].

The fundamental matrix F only depends on projective properties of the camera matrices P and P'. These camera matrices relate three dimensional space measurements to image measurements and thus they depend both on the image coordinate frame and the choice of the world coordinate frame. However, F doesn't depend on the choice of the world coordinate frame. A change on this coordinate frame will change P and P' but it will not change F. So, it's possible to affirm that F is unchanged by a projective transformation of three dimensional space. This leads to an important result: if H is a 4x4 matrix representing a projective transformation of three dimensional space, then the fundamental matrices of the pairs of camera matrices (P, P') and $(PH, P'H)$ are the same [53].

Hence, although a pair of camera matrices (P, P') uniquely determine a fundamental matrix F, the inverse is not true. The camera matrices can be determined from fundamental matrix up to a projective transformation [53]. To remove this ambiguity and obtain the true pair of camera matrices is necessary to do more steps that will be described in subsequent sections.

Because of the ambiguity explained here, usually is defined a canonical form of the camera matrices. In this form the first matrix is of the simple form $[I|0]$, where I is the 3x3 identity matrix and 0 is a null 3-vector [53].

As seen before, knowing F it's possible to determine the pair of camera matrices up to a projective transformation of three dimensional space. The pair of camera matrices in canonical form corresponding to a fundamental matrix F can be computed in the following way: $P = [I|0]$ and $P' = [[e'] \times F|e']$, where e' is the epipole such that $e'^T F = 0$ [53].

In this work, the computation of camera matrices from fundamental matrix was performed using the code provided by [54]. This code is based in the theory described before. It takes as input the fundamental matrix and retrieves the camera matrices in canonical form.

Calibration

In order to remove the ambiguity described in the previous section and obtain a true Euclidean reconstruction is necessary to perform the calibration of the x-ray imaging system. This is an essential step in 3D reconstruction because it will help clarify the relation between 2D image and 3D space by determining the geometrical parameters of the radiographic setup [55, 56].

The x-ray imaging system can be described through a pinhole camera model. This type of camera model describes the mathematical relationship between the coordinates of a 3D point and its projection onto the image plane of an ideal pinhole camera. This is the simplest camera model where the camera aperture is described as a point (pinhole) and no lenses are used to focus light [57]. The light travels from a point along a single straight line through the pinhole onto the image plane [58]. This camera model does not include some effects that occur in most real cameras, like geometric distortions or blurring of unfocused objects that happen when lenses and finite sized apertures are present. The omission of these phenomena in the pinhole camera model means that it can only be used as a first order approximation of the mapping from a 3D scene to a 2D image [58].

However some of these effects can be compensated, for example by applying suitable coordinate transformations on the image coordinates, and other effects are sufficiently small to be neglected if a high quality camera is used. Thus, the pinhole camera model often can be used as an acceptable description of the relation between 2D image and 3D space, for example in computer vision and computer graphics [59].

In Figure 3.8 it's possible to observe a representation of the x-ray imaging system as a pinhole camera model [60]. In this representation $R = (O, X, Y, Z)$ is the object coordinate system and in the case of an x-ray system, the object is the body part that is being x-rayed. $R_1 = (S_1, X_1, Y_1, Z_1)$ and $R_2 = (S_2, X_2, Y_2, Z_2)$ are the coordinate systems of the two x-ray sources with S_1 and S_2 the corresponding positions of those sources. The xy planes of these coordinate systems are parallel to the corresponding uv image planes [60].

Equation 3.1 describes the relation between a 3D object point and its projections onto the left and right image planes. This relation can be modelled as two linear transformations using homogeneous coordinates with 3 × 4 matrices M_1 and M_2 representing, respectively, the calibration

matrices of the left and right systems [60].

$$\begin{bmatrix} w_i.u_i \\ w_i.v_i \\ v_i \end{bmatrix} = M_i \begin{bmatrix} X \\ Y \\ Z \\ 1 \end{bmatrix} \text{ for } i = 1, 2, \tag{3.1}$$

In this equation w denotes a scaling factor and (u, v) denotes the image coordinates of a 3D point $(X.Y, Z)$.

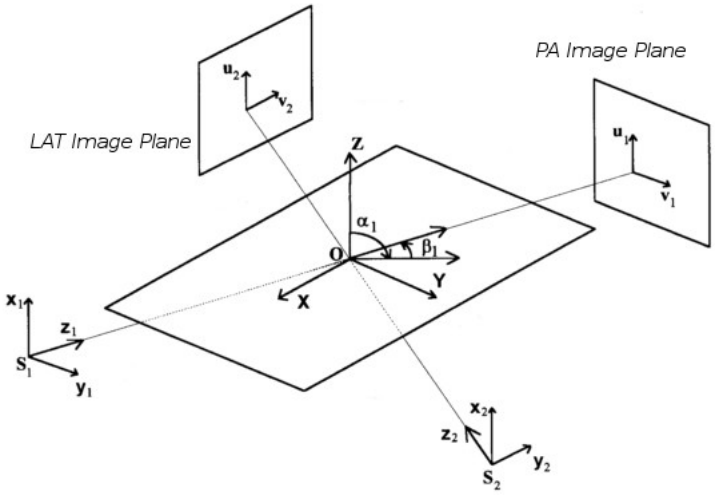

Figure 3.8: Representation of radiographic setup through pinhole camera model

The calibration matrices M_i can be described with the geometrical parameters [60]. So, the matrices M_i can be decomposed in the following way:

$$M_i = P(d_i, s_p, u_{Si}, v_{Si})D_i \text{ for } i = 1, 2, \tag{3.2}$$

In equation 3.2 s_p denotes the pixel size, d_i denotes the distance from source S_i to the image plane, (u_{Si}, v_{Si}) denote the projection image coordinates of the source S_i or the principal point. This parameters are also called the intrinsic parameters of the camera and so P is the intrinsic camera matrix [61]. This matrix represents the linear transformation in homogeneous coordinates associated with the perspective projection of a 3D point on the image plane. D_i is the matrix describing the displacement from the object coordinate system $R = (O, X, Y, Z)$ to the source coordinate system $R_i = (S_i, x_i, y_i, zi)$ [60], that is the transformation from object coordinates

to camera coordinates. This transformation is defined by the extrinsic parameters, namely rotation and translation, and thus can be described in the following equation [60]:

$$D_i = T_Z(d_{Si})R_Y(\beta_i)R_X(\alpha_i) \tag{3.3}$$

So $(\alpha_i, \beta_i, d_i, d_S, u_{Si}, v_{Si})_{i=1,2}$ denote the geometrical parameters that need to be estimated in the calibration step [60].

Once this step is done it's possible to triangulate the points and obtain its 3D coordinates in the real coordinate system.

Most of the methods to perform the calibration of x-ray systems make use of calibration objects. These objects can be simply a coin or a spherical object (stell ball) or can be more complex like a vest or a calibration phantom composed by a set of steel pellets with known 3D coordinates [62].

In these methods, first the 2D coordinates of the pellets are identified on the x-ray images, manually or automatically. The 3D coordinates of these pellets are known a priori so using the correspondences between the 3D and 2D coordinates it's possible to obtain the geometrical parameters of the x-ray imaging system [61].

Some problems associated with these methods are the size of the calibration objects that usually are very large in order to contain the anatomical structures that are being reconstructed [63].

Also, the patient motion between the exposures will create inconsistencies between the calibration and patient stereo geometries and thus the reconstruction algorithm will be vulnerable to this motion. So, in these cases it's necessary to use a rotatory platform in addition to the calibration object [64].

So, these methods have not found widespread clinical use because the physicians understand that the use of a calibration object would disturb the already quite complex clinical protocol for the acquisition of x-ray images [60].

The disadvantages related with the calibration objects caused the appearance of self-calibration methods. In these type of calibration the use of a calibration object is eliminated.

In these type of methods, the problem of finding the geometrical parameters is described as a minimization problem where the objective is to minimize landmark reprojection errors [64]. It's necessary to provide an initial guess for the geometrical parameters and two point sets that correspond to observed and analytical projections of a set of N reference points of unknown 3D coordinates. The minimization algorithm will minimize the mean square distance between these two point sets [60].

However these methods aren't able to determine scale which makes impossible to perform

absolute measures, like length of bones. To overcome this issue, a calibration object can be used. This object can also be used to determine the initial guess for the geometrical parameters [63].

In this work, it was implemented the self-calibration method described in [60].

This method uses an iterative process and an initial guess for each geometrical parameter to solve the minimization problem and find the best estimation for the geometrical parameters [60].

Using equations 3.2 and 3.3 it's possible to decompose the calibration matrices as follows [60]:

$$M_i(\xi_i) = P(d_i, s_p, u_{Si}, v_{Si}) T_Z(d_{Si}) R_\gamma(\beta_i) R_X(\alpha_i), \tag{3.4}$$

where $\xi_i = (\alpha_i, \beta_i, d_i, d_S, u_{Si}, v_{Si})_{i=1,2}$ denote the geometrical parameters of the x-ray imaging system that will be estimated [60].

The coordinates of the analytical projections $(u_{n,i}(\xi_i, p_n), v_{n,i}(\xi_i, p_n))_{i=1,2}$ of the 3D object points $p_n = (X_n, Y_n, Z_n)$ can be computed from equations 3.1 and 3.4 [60].

The coordinates of the observed projections of reference points $(u_{n,i}, v_{n,i})_{i=1,2}$ are identified manually in both views [60]. In this work, the observed projections and the 3D object points were identified by the method described previously in the subsection Extraction of anatomical landmarks/-contours. Then, the coordinates of the analytical projections of the 3D object points were computed as described before.

In order to estimate the geometrical parameters it's necessary to define the criterion that needs to be minimized. In this case, the criterion is the following [60]:

$$\varepsilon(\xi) = \sum_{n=1}^{N} \sum_{i=1}^{2} d[(u_{n,i}^m, v_{n,i}^m), (u_{n,i}(\xi_i, p_n), v_{n,i}(\xi_i, p_n))]^2 \tag{3.5}$$

In equation 3.5, $\xi(\xi_1, \xi_2)$ denote the geometrical parameters for the left and right views, $d[]$ denotes Euclidean distance, $(u_{n,i}^m, v_{n,i}^m)$ denote the measured projection coordinates of the reference points in the both views. Knowing the initial guess for the geometrical parameters and the observed and computed projection coordinates, the geometrical parameters are estimated with an iterative process where a correction for the parameters is computed. In each iteration, this correction is used to update the parameters and the new updated parameters are used as an approximation for the next iteration. This iterative process is repeated until the correction or the criterion become negligible [60].

The correction for the geometrical parameters can be computed using numerical methods. In this work, the Levenberg-Marquardt algorithm was used as suggested in [60]. This is a standard

technique used to solve non-linear least squares problems [65]. These type of problems occur when trying to fit a parametrized function, that is not linear in the parameters, to a set of measured data points by minimizing the sum of the squares of the errors between the data points and the function. The methods to solve this type of problems try to reduce the sum of the squares of the errors by iteratively improving the parameter values [66].

In this work, the Levenberg-Marquardt algorithm was implemented using the dlib C++ library. This algorithm was adapted to the problem of finding the best estimation for the geometrical parameters. In this case, the camera matrices obtained through the method described in the previous section were used as the initial guess.

Triangulation

Now, that all the concepts necessary were explained in the previous sections, the triangulation technique will be described.

The triangulation problem can be described as the problem of finding the position of a point in 3D space given its position in two images. The images are taken with cameras with known calibration and pose. From the coordinates of the point in both images and the two camera matrices is possible to compute the rays in space corresponding to the two image points. As it was seen in Epipolar Geometry section, the point in 3D space corresponding to the two image points will be located in the intersection of the rays back-projected from image points. With this, the triangulation problem boils down to find the intersection of these two lines in the space [67].

This problem appears to be trivial, however in the presence of noise it's not guaranteed that the rays will meet. So, it's necessary to find the best point of intersection [67]. This is done through the definition and minimization of a cost function [53].

The two rays corresponding to a matching pair of points $u \leftrightarrow u'$ will meet in space if and only if the points satisfy the epipolar constraint: $u'^T F u = 0$. However, in the presence of noise, the point correspondence will be noisy and will not satisfy this epipolar constraint. This noise is due to digitization errors or to errors in the identification of the points. In this case, $\widehat{u} \leftrightarrow \widehat{u'}$ will be the correct values of the corresponding image points. These points lie close to the measured points $u \leftrightarrow u'$ and satisfy the epipolar constraint $\widehat{u'}^T F \widehat{u} = 0$ [67].

So, the objective in the triangulation problem, is to find the points $\widehat{u}$ and $\widehat{u'}$ that minimize the function [67]:

$$d(u, \widehat{u})^2 + d(u', \widehat{u'})^2, \tag{3.6}$$

where $d(,)$ denotes Euclidean distance. This function is a sum of squared distances.

There are several methods to perform triangulation through the minimization of equation 3.6. One of them is the polynomial method. In this method, equation 3.6 is reformulated to [67]:

$$d(u, \lambda)^2 + d(u', \lambda')^2, \tag{3.7}$$

where λ and λ' range over all choices of corresponding epipolar lines. This reformulation it's possible because the optimum point $\widehat{u}$ lies on the epipolar line λ and the corresponding point $\widehat{u'}$ lies on the epipolar line λ'. Also, any pair of points lying on the epipolar lines λ and λ' will satisfy the epipolar constraint. The points $\widetilde{u}$ and $\widetilde{u'}$ corresponding to the epipolar lines λ and λ' respectively, lie closest to the measured points u and u'. So, these points will minimize equation 3.6 and thus $\widehat{u} = \widetilde{u}$ and $\widehat{u'} = \widetilde{u'}$, with $\widetilde{u}$ and $\widetilde{u'}$ defined with respect to the pair of epipolar lines λ and λ'. From this, it's possible to say that $d(u, \widehat{u}) = d(u, \lambda)$ and $d(u', \widehat{u'}) = d(u', \lambda')$, with $d(u, \lambda)$ and $d(u', \lambda')$ representing the perpendicular distances between the points u, u' and the lines λ, λ'. From this last result, it's possible to reformulate equation 3.6 in equation 3.7 [67].

The strategy to solve the minimization problem can be the following [67]:

- Parametrize the family of epipolar lines in the first image by a parameter t. So an epipolar line can be written as $\lambda(t)$ for the first image
- Compute the corresponding epipolar line $\lambda'(t)$ for the second image, using the fundamental matrix
- Write the function to minimize as a function of t, $d(u, \lambda(t))^2 + d(u', \lambda'(t))^2$
- Find the value of t that minimizes this function

It's possible to see that with this strategy, the problem is reduced to find the minimum of a function of a single variable, t. Using techniques of elementary calculus, this problem reduces to finding the real roots of a polynomial of degree 6 [67].

Another way to perform triangulation is through the Poly-Abs method. This method is an adaptation of the polynomial method described before. In Poly-Abs instead of minimizing the sum of squared distances, it's minimized the sum of absolute values of the distances [67].

Other method to perform triangulation is the linear method that is the most common one. In this method, supposing $\mathbf{u} = Px$, where in homogeneous coordinates $\mathbf{u} = w(u, v, t)^T$. (u, v)

are the observed point coordinates and w is an unknown scaling factor. The equation $\mathbf{u} = Px$ can be written in the form [67]:

$$wu = p_1^T x, wv = p_2^T x, w = p_3^T x, \tag{3.8}$$

where p_i^T denotes the i-th row of the camera matrix P.

Using the third equation, it's possible to eliminate w from the first two equations and get the next result [67]:

$$up_3^T x = p_1^T x, vp_3^T x = p_2^T x \tag{3.9}$$

Joining the information of the two views, 4 linear equations in the coordinates of x are obtained and they can be written in the form $Ax = 0$, with A a 4x4 matrix. These equations will define x up to an indeterminate scale factor. In the presence of noise, the equations will not be satisfied precisely, so instead of finding the exact solution, the best solution is searched [67].

It's possible to solve x for $Ax = 0$ in two different ways. The first is the Linear-Eigen method and this method tries to find x to minimize $\|Ax\|$ subject to the condition $\|x\| = 1$. So, the solution for this problem will be the unit eigenvector corresponding to the smallest eigenvector of the matrix $A^T A$. And the solution can be found using SVD [67].

The second method is the Linear-LS method. In this method assuming that $\mathbf{x} = (x, y, z, 1)^T$ will reduce the set of homogeneous equations $Ax = 0$ to a set of 4 non-homogeneous equations with 3 unknowns. Then, it's possible to find a least-squares solution using the method of pseudo-inverses or using SVD [67].

There is another class of triangulation methods that are the iterative ones. The linear methods described before can be inaccurate because the value being minimized $\|Ax\|$ has no geometric meaning and don't correspond to the function 3.6. Also, if the equations, corresponding to the rows of A, are multiplied by some weight, the solution will change. So, the solution to this will be the iterative linear method because in this case, the weights of the linear equations will be changed in a way that the weighted equations correspond to the errors in the measurements of image coordinates [67].

This iterative method can be applied both to the Linear-LS and Linear-Eigen methods. The last triangulation method described in this work will be the mid-point method. This may be the simplest method because it's easy to compute. However, concerning to results, it's the worst of all the methods described here. It consists in finding the mid-point of the common perpendicular to the two rays corresponding to the matched points [67].

The triangulation method used should be invariant to affine or projective transformations in space. This is important because in affine and projective reconstruction there is no meaningful metric information about the object space [53]. The Polynomial and Poly-Abs methods are affine and projective invariant. The mid-point, Linear-Eigen and Iterative Linear-Eigen methods are neither affine nor projective invariant while the Linear-LS and Iterative Linear-LS methods are affine invariant [67].

In these type of reconstruction methods, the 3D scene is reconstructed up to an unknown transformation (affine or projective). In these cases, normally the correct pair of camera matrices are not known. Instead a pair PH^{-1} and $P'H^{-1}$ is known where H is an unknown transformation. The triangulations results in these cases don't correspond to a true Euclidean reconstruction [53]. In order to obtain such a reconstruction it's necessary to calibrate the imaging system as it was described in the previous section.

In this work, prior to the triangulation of the detected edge points, it was necessary to perform the correspondences between the detected edge points. This was performed using the *Flann Matcher* provided in the OpenCV library. With this matcher, 778 point correspondences were detected.

The triangulation step was performed using two different techniques, in order to compare the results from both and choose the most appropriate technique. So, it was used the function triangulatePoints from the library OpenCV and an implementation in C++ of the Iterative Linear-LS method provided in [68]. The OpenCV function takes as inputs the two camera matrices and the two arrays of the corresponding points identified in the two images. It retrieves an array with the reconstructed points in homogeneous coordinates. The Iterative Linear-LS method takes as inputs the two camera matrices, the two arrays of the corresponding points, the matrix of the intrinsic camera parameters and the transpose of this matrix and the matrix of distortion coefficients. It outputs an arrays with the reconstructed points in cartesian coordinates and the reprojection error.

The results for the triangulation step gave a reprojection error of 39.7383 for the Hartley and Zisserman method and a reprojection error of 248.616 for the OpenCV method.

As we can see Hartley and Zisserman method produced the lowest reprojection error and for that reason this was the method selected to perform the triangulation.

3.2.3 Correspondences

After the 3D reconstruction of image points, the transformation necessary to apply in the generic model is computed. This transformation is computed by the comparison between the 3D reconstructed points and the points identified in the generic model. In order to perform this comparison,

it's necessary to first settle the correspondences between the two point sets. In this section will be described the method implemented to perform this correspondence.

The correspondence between points was implemented in this work using the Point Cloud Library (PCL). It was used the function to determine correspondences of the class CorrespondenceEstimation. This class belongs to the Registration API of 3D. The function used takes as inputs the two point clouds and retrieves the indices in the two point clouds of the corresponding points.

The final result was a number of 778 point correspondences between the triangulated points and the detected edge points of the 3D model.

3.2.4 Transformation Computation

After the establishment of the correspondences, the transformation between the two point sets was computed. This was done using the thin-plate spline interpolation.

The term TPS refers to a physical analogy that involves the bending of a thin sheet of metal. In image warping applications, TPS involves the minimization of a bending energy function for a transformation over a set of given landmark points [69].

The bending energy function to minimize will be the following [69]:

$$\iint_{R^2} \left(\left(\frac{\partial^2 z}{\partial x^2} \right)^2 + 2 \left(\frac{\partial^2 z}{\partial x \partial y} \right)^2 + \left(\frac{\partial^2 z}{\partial y^2} \right)^2 \right) dxdy \tag{3.10}$$

The thin-plate spline can be used to solve an interpolation problem, in this case, the computation of a map $R^3 \rightarrow R^3$ relating the two point sets [70]. This map will relate the two points sets and thus will give the transform that it's necessary to apply in the generic model.

To perform the TPS interpolation it was used the Thin-Plate Spline Kernel Transform provided by ITK Library. In this implementation, the matrix of the transform is computed from the corresponding points of the two point sets.

3.2.5 Model deformation

The last step of the reconstruction process is the deformation of the model. The model is deformed with the transformation computed in the previous step. The expected final result it's a deformed model that matches the original radiographic images.

The transform computed in the previous step is the result of the comparison between the two

point sets. The differences between each pair of points will be the transformation that needs to be applied in the moving point, that is the point of the generic model, so that it will fit the fixed point, that is the 3D reconstructed point. In the end, we will have the transformations necessary to apply to each point of the generic model so that it will fit the 3D reconstructed points. In this step, the application of the transformation computed to the generic model is performed.

To perform this step, the Transform Mesh Filter of ITK Library was used. This filter takes as input the initial mesh and the matrix of the transform to be applied and outputs the final deformed mesh.

The final result of this step is represented in Figure 3.9

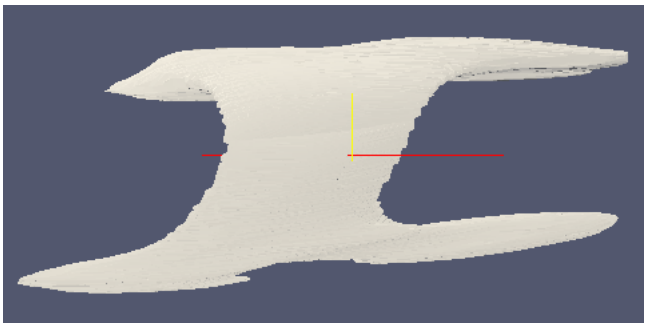

Figure 3.9: Final 3D model of the femur

3.3 Reconstruction method with extracted edge points

The results obtained using the method described before weren't very accurate. Because of these poor results, it was decided to develop a different method. This method doesn't perform the triangulation of points, instead it computes the transformation necessary to apply in the generic model only using 2D points extracted from the patient's radiographic images and the generic model's radiographic projections. So, this new method performs most of the computations in the 2D space which is an advantage because it's easier to work in this space since the original radiographic images belong to this space. Also, the triangulation process could be the main source of error in the previous method because it involves some parameters that are related with the camera and in this work those parameters where not known and had to be estimated. So, the triangulation was not an accurate process and could be leading to errors in the reconstruction process. Since, this new method doesn't perform the triangulation of points it can lead to better results. The workflow

of this method is detailed in the diagram presented in Figure **??**.

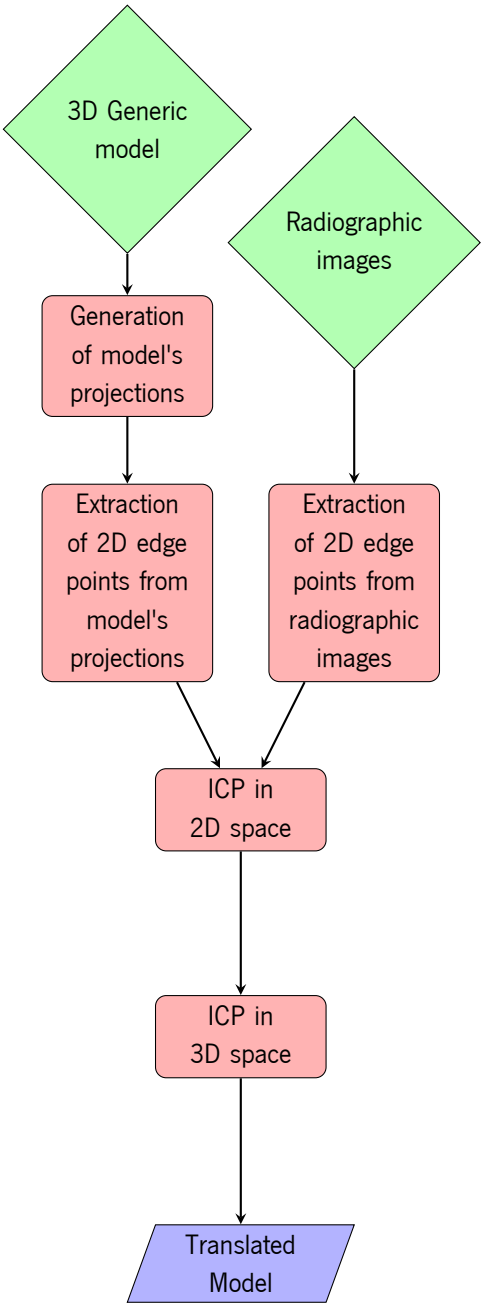

(a) Flow Chart of first part of reconstruction method with extracted edge points

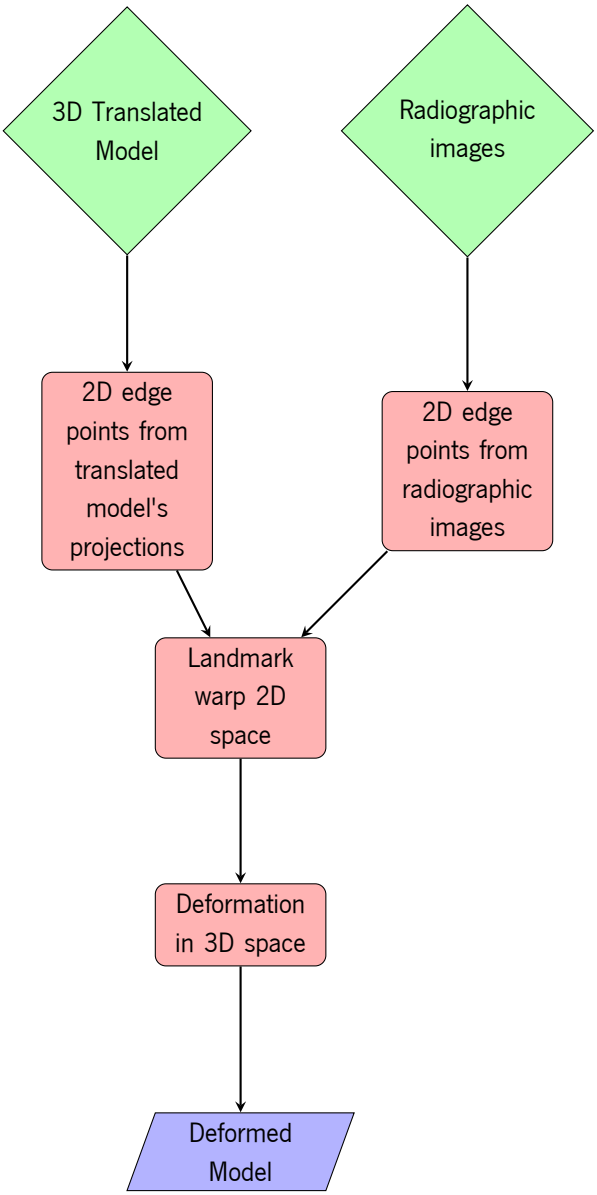

(b) Flow Chart of second part of reconstruction method with extracted edge points

3.3.1 Generate model's radiographic projections

The first step of the method was the generation of the generic model's radiographic projections. These projections will simulate two orthogonal x-rays and will be used to compare with the patient's radiographic images. This was performed using the example code *GenerateProjection* belonging to the application *IntensityBased2D3DRegistration* that is available in the ITK Apps Repository.

In this example code it's necessary to provide the 3D model and the values for the focal length, translation and rotation. To generate the frontal radiographic projection it was used a focal length of 1000 mm, a translation of $t = [-150, -400, 0]$ and a rotation of 180 degrees around x. The center of rotation was setted to $c = [173.5, 340.5, 0]$ and the size of the projection image was defined as $size = [347, 681]$ so that the projection image will have the same size as the original radiographic image. To generate the lateral radiographic projection, the value for focal length was 100000 mm, the translation was $t = [-100, -245, -110]$ and it was applied a rotation of 90 degrees around y. The center of rotation and size were the same used for the frontal projection.

In Figure 3.11, it's possible to observe the generated model's radiographic projections. In Figure 3.11a it's present the frontal projection and in 3.11b the lateral projection.

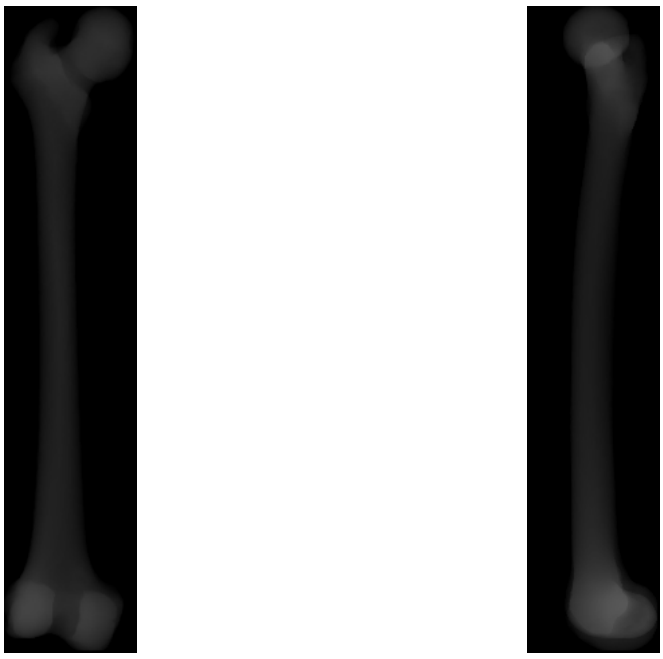

(a) Frontal projection (b) Lateral projection

Figure 3.11: Model's radiographic projections

3.3.2 Edge extraction

The second step of the method is to extract the edge points both on the patient's radiographic images and the model's radiographic projections. Then, these points will be matched and compared in order to obtain the deformation that is necessary to perform to obtain the patient's specific 3D bone model.

The detection of edge points was performed using the Canny Edge algorithm as described before. The parameters' values used for the projection images were:

- $variance = 20;$
- $upperThreshold = 9;$
- $lowerThreshold = 0;$

And for the radiographic images were:

- $variance = 10;$
- $upperThreshold = 8;$
- $lowerThreshold = 0;$

In Figure 3.12, the detected edges can be observed. In Figure 3.12a it's presented the detected points on the model's projection and in Figure 3.12b on the patient's radiographic images. Both images are correspondent to the frontal radiographic image.

3.3.3 Iterative Closest Point 2D

The first step to fit the model to the patient's radiographic images is to perform a rigid transform. With this transform the generic model will be aligned with the original radiographic images.

So, after the detection of the edge points in all images, it's necessary to compute the correspondences between the points of patient's radiographic images and model's projections. These correspondences will be used to compute the rigid transformation that needs to be applied in the points from model's projections so that they will fit the points from patient's radiographic images. This was performed using the ICP algorithm provided by the ITK Library.

The ICP algorithm is used to minimize the differences between two point sets. One of the point set is the reference, so its points will be kept fixed. The other one is the source, so this will

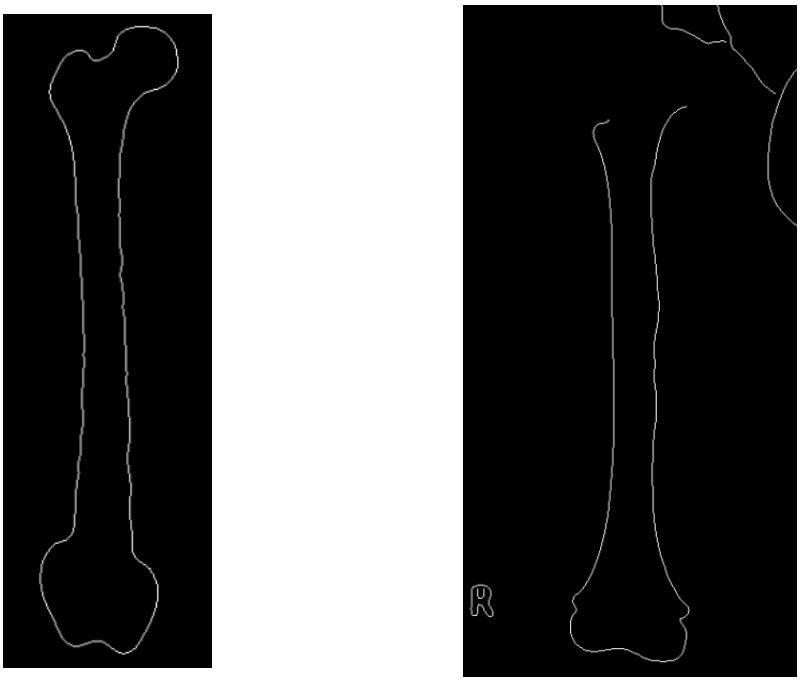

(a) Frontal edge points of model's projection

(b) Frontal edge points of patient's radiographic image

Figure 3.12: Detected edge points on the frontal model's projection and patient's radiographic image

be transformed in order to match the reference point set. The transformation computed with this algorithm is rigid, it can be a combination of translation and rotation. This transformation will be iteratively updated in the algorithm in order to minimize the distance between the source and the reference point sets [71].

The main steps of the algorithm are presented in Figure 3.13.

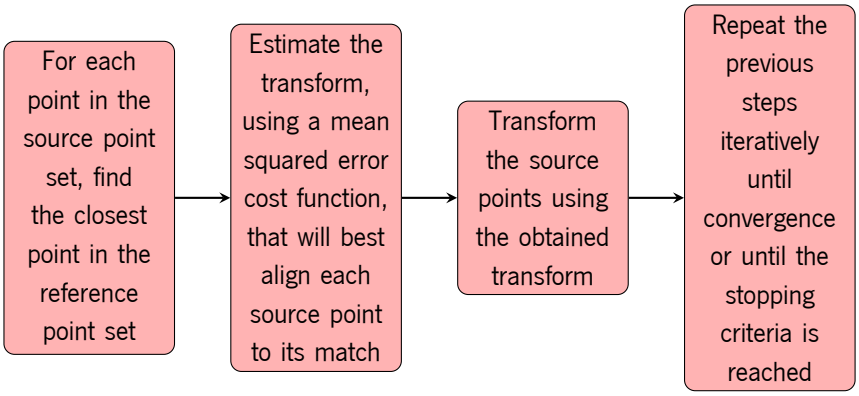

Figure 3.13: Flow Chart of ICP algorithm

So, this algorithm computes the correspondences between the points and also the transform to apply to each point of the moving point set so that they will fit the points of the fixed point set [71]. In this case, the fixed point set are the edge points of the original radiographic images and the moving point set are the edge points of the model's projections. The execution of this algorithm outputs a transform and the point correspondences. Then, the resulting transform will be applied to each point of the moving point set. At the end of this step, we have the point correspondences between the two point sets and the transformed points of the moving point set.

In Figure 3.14 it's possible to observe the detected edge points with the Canny Edge algorithm of both images and the final transformed points. All these points were superimposed in the frontal original radiographic image. The blue points are the detected edge points of the radiographic image, the green are the detected edge points of the model's projection and the red are the transformed points of the model's projection.

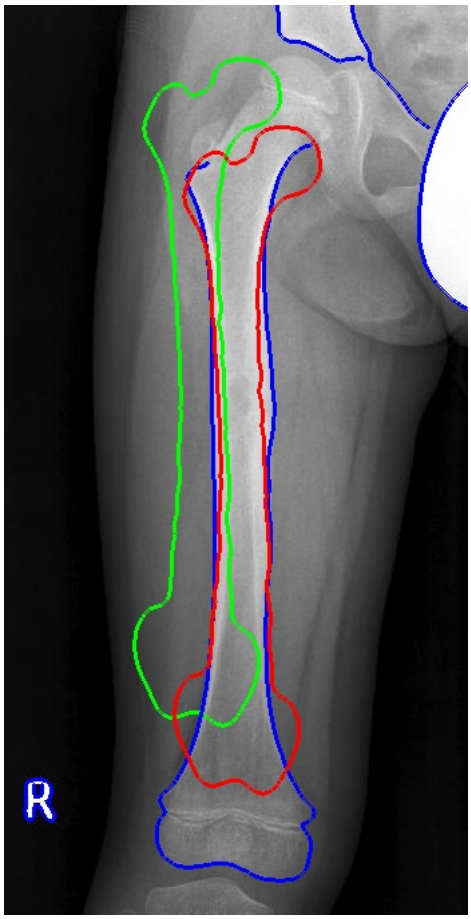

Figure 3.14: Detected and transformed edge points

3.3.4 Iterative Closest Point 3D

In the previous step, a rigid transform was computed. However, this transformation was calculated basing in the 2D points of the images, so the final result is a 2D transform that can be applied to the 2D points. But, to apply the transform in the generic model, a 3D transform is needed.

The strategy applied in this work, was to create a 3D transform by adding the z component to the 2D transformed points resulting from the previous step. The value attributed to z corresponded to the z-value of the generic model's center. So, with this, it's possible to compute a 3D transform that will be applied in the center of the model.

Once again, the ICP algorithm was applied, but in this case, it's applied in the 3D space and the moving point set are the generic model's points and the fixed point set are the transformed points with the z-value equal to the model's center. With this algorithm, a rigid 3D transform will be computed. This transform will be applied to all the model's points, which will cause a translation in the model.

The transform computed with the ICP algorithm is applied to the model using the Transform Mesh Filter from ITK Library. This filter applies a transform to all the points of a mesh. The additional content of the mesh, like connectivity or additional information on cells or points, is passed untouched. The inputs of this filter is a mesh and a transform and the output will be the transformed mesh. In this case, the inputs are the generic model and the 3D rigid transform computed with ICP and the output will be the transformed generic model.

The final result of this step, is the generic model aligned with the original radiographic images.

In Figure 3.15, it's possible to see the generic model and the radiographic image before the translation and in Figure 3.16, after the translation.

3.3.5 Landmark warping in 2D

After the rigid transformation, the generic model is aligned with the patient's radiographic image. So, the next step, is to deform the model so that it will fit the patient's specific anatomy.

As before, first the deformation was computed in the 2D space using the points of the projections transformed with the ICP algorithm and the corresponding points of the radiographic images. This was performed using the class *DeformationFieldSource* from ITK Library.

This class computes a deformation field from two sets of landmarks. One set is associated to the input space (fixed point set) and the other to the output space (moving point set).

The two point sets will be compared in order to determine the deformation that needs to be

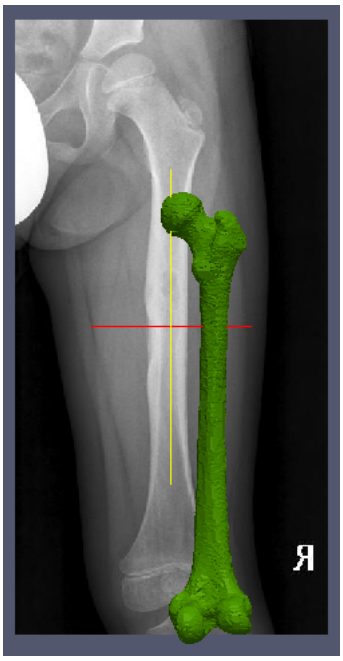

Figure 3.15: Initial generic model and patient's radiographic image

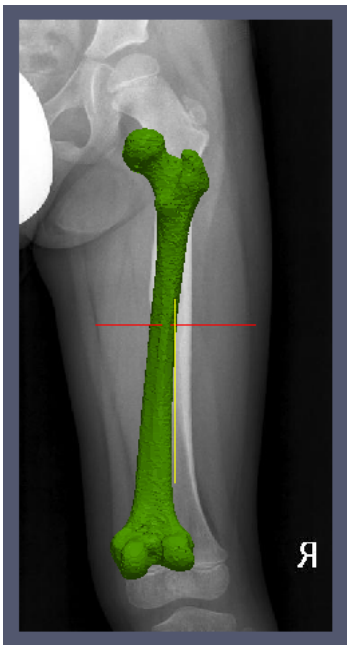

Figure 3.16: Generic model after ICP algorithm and patient's radiographic image

applied in each point of the output set so that it will fit the input set. The deformation values are computed and interpolated using a Kernel Based Spline. One important factor in the Kernel Based Spline is the number of landmarks. This parameter will have an important effect on both the precision of output deformation field and the computational time required for the filter to complete the estimation.

The output will be a deformation field that is a image with the same size, origin and spacing of the output space and each pixel has the corresponding deformation value. The pixel type of the deformation field is vector, because the deformation values correspond to vectors with the direction and intensity of the deformation. When the deformation field is applied to the moving image, this will be deformed by adding the corresponding displacement at every point of the point set.

In this case, the moving point set are the 2D transformed points and the fixed point set are the corresponding edge points of the radiographic image.

At the end of this step, a deformation field is obtained and this will be applied to the transformed points. The result will be a set of deformed points that will be used in the next step to deform the generic model.

In Figure 3.17, it's possible to observe the transformed points in red and the deformed points in green. The edge points of the radiographic image were also drawn but the deformed points superimposed these points. This shows that the deformation was computed correctly because the final deformed points correspond to the points of the original radiographic image.

3.3.6 Deformation of 3D model

Once again, it was necessary to apply the deformation computed before to the generic model. In order to do this, it's necessary to convert the 2D deformation to the 3D space. This was done using the same method as before, that was add the z-value to the deformed points and this value as equal to the center of the model. Then, the ICP algorithm was used again, giving a transform that will be applied to the generic model's points. However, despite the 2D points were transformed using a non-rigid transformation, which means they were deformed, the ICP algorithm computes only a rigid transformation which means that the points of the model won't be deformed and will suffer again only a translation. So, the deformation computed in the 2D space will not be converted to the 3D space using the ICP algorithm. Thus, the generic model will not suffer any deformation, will only suffer rigid transformations.

The resulting model can be observed in the Figure 3.18.

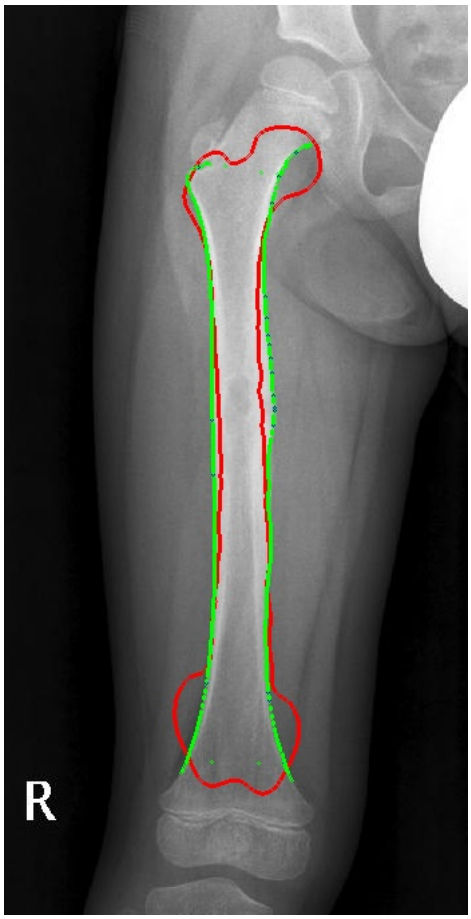

Figure 3.17: Deformed and transformed edge points

It was made an attempt to use an algorithm to perform the deformation of the generic model. It was used the *WarpMeshFilter* provided in the ITK library. This filter takes as input a mesh and a deformation field and outputs the deformed mesh. However, when using this filter it appears that nothing happen, the final model was exactly the same as the initial model. So, in order to test if the algorithm was working correctly, it was created a random deformation field. Then, it was used the *WarpMeshFilter* with the generic model and the random deformation field. The final mesh was a translated mesh, which is not correct because this algorithm should apply a non rigid transformation in the mesh and translation is a rigid transformation. Thus, the problem of deformation seems to be related with the algorithm used.

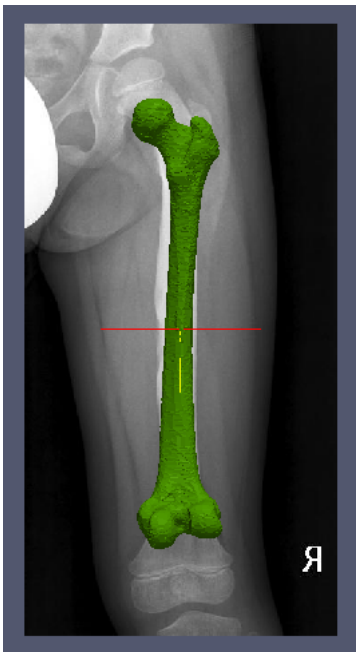

Figure 3.18: Generic model after deformation

3.3.7 Scale Transform

The next step in the reconstruction process, is to resize the generic model so that it will fit the length of the bone present in the original radiographic images.

This was performed using the Scale Transform provided by ITK Library.

To compute the transform it's only necessary to set the scale and the center.

In order to compute the scale, the total length of the bone was measured both on the original radiographic images and on the generic model. The scale to apply on the model was obtained through the comparison of these lengths. The calculated scale was 1.28125 and this corresponds to the y-value because we want to scale the length of the bone that is in the y axis.

The center was setted to the center of the generic model, in order to scale the model from the center. The coordinates of the center were $c = [178, 348, -250.5]$.

After the computation of the scale transform, this was applied to the generic model using the Transform Mesh Filter from ITK Library in the same way as described before.

The result of the application of this transform can be seen in Figure 3.19.

This is the last step of this method, so here the final 3D bone model is obtained.

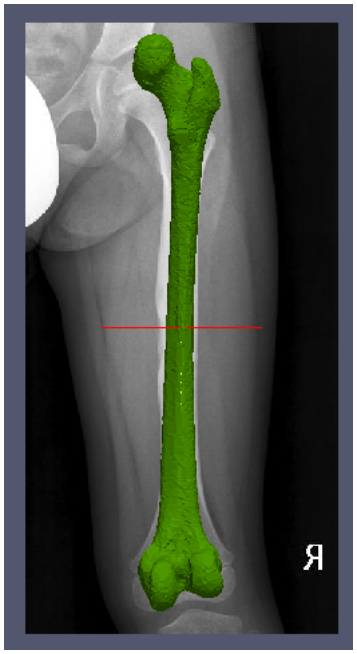

Figure 3.19: Generic model after scale transform

Chapter 4

Discussion and Conclusions

4.1 Discussion

4.1.1 Reconstruction method with triangulation of anatomical landmarks

The results obtained with the first method were very poor. One of the main reasons of the poor results is the lack of information about the x-ray imaging system. This information is crucial for the triangulation algorithm that is used in this method. If this information is not known precisely, the calibration of the x-ray system will not be accurate and the triangulation process will give poor results. The information needed for the calibration process is the focal distance (distance from source), principal point and the rotation and translation between cameras. Without this information, it's only possible to perform an estimation for the calibration. Because the estimation of calibration parameters is an iterative process it is necessary to provide an initial estimation of those parameters to initiate the process. This initial estimation needs to be an approximation of the final parameters in order to the iterative process converges and give good results. However, in this work an approximation of the initial calibration parameters is not available, instead it was used some parameters found on the literature, so this can be the cause of the bad results of the calibration process. Another reason is the fact that without knowing the calibration it's not possible to perform a true Euclidean reconstruction, it's only possible to have a projective reconstruction. So, the computed pair of camera matrices differ from the true ones by an unknown transformation H [67]. To transform the obtained projective reconstruction in a true Euclidean reconstruction it's necessary to find the trans-

formation H. This can be accomplished by using ground control points, that are points with known 3D coordinates in an Euclidean world frame and with known 2D coordinates in the radiographic images. With the 3D coordinates of these points it's possible to compute the transformation H and obtain a true Euclidean reconstruction and so it's possible to obtain the real 3D coordinates of the radiographic image's points [53]. However, in this work, this was not possible to accomplish because a radiographic imaging system was not available, all the images used in this work were obtained from medical databases available online. Without this system, it is not possible to have ground control points to compute the transformation.

Another issue that can be related to the weak results of this method is the point correspondence step. This step is performed before the triangulation and is done to match the points from the two orthogonal images. The method used here to find the correspondences is based on the intensities of the images and this may not be appropriated for this case. This is because the intensities of a radiographic images are higher in the bone parts, and so all the bone parts will have more or less the same intensity, thus pixels that correspond to the upper bone in one image can be corresponded to pixels of the lower bone in the other image. So, to perform the correspondences between the images we have to take in account not only the intensities of the images but also the anatomical shape of each bone. In this work, this was not performed because it was not encountered a suitable algorithm to perform this task. This can be a task to perform in the future in order to enhance the results of this method. Also, the two orthogonal images in comparison are very different, so it is hard to find correspondences and sometimes the correspondences found are not true. All these issues will lead to erroneous correspondences that will feed the triangulation algorithm and once again lead to bad results. The failure of the correspondence step may be the principal reason that the final model appears to be without thickness.

The previous work done in this area [6, 34–37] achieved better results mainly because the calibration was performed correctly and so the triangulation process was successful. This calibration was performed using a calibration object or with a priori knowledge of the calibration parameters of the radiographic system used to acquire the images. In the case of this work, this couldn't be done because no radiographic system was available, so it wasn't possible to know the calibration parameters of the system and also a calibration object wasn't disposable. Thus, it wasn't possible to perform the calibration of the system correctly, it was only possible to estimate the parameters which introduced errors in the process. Also, the calibration object allows to have the 3D coordinates of the steel balls in the real world and these can be used as ground control points to obtain a true Euclidean reconstruction.

One way to have better results with this method, is, as said before, to perform the calibration of the system. This can be done by using a calibration object during the acquisition of the exams. Usually, this object is composed by acrylic plates and steel balls. In the radiographic image, the steel balls will appear and knowing their positions in the image and in the 3D world, it's possible to obtain the calibration parameters and calibrate the system. With this calibration, it's possible to obtain a true Euclidean reconstruction and thus the triangulation with achieve better results. If the triangulation is successful then the overall results of the method will be enhanced, because the triangulation gives the 3D coordinates of identified points on the radiographic images and with these points it's possible to extract the surface of the 3D bone model. Once this surface is extracted, we have the final patient's specific 3D bone model. An alternative to the surface extraction is to use the 3D coordinates resulting from triangulation and compare them to the edge points of the generic model. From this comparison will result the transformation that needs to be applied in the generic model so that it will fit the patient's radiographic images.

4.1.2 Reconstruction method with extracted edge points

The second method improved the results obtained. With this method it's possible to obtain a 3D bone model that can truly correspond to a real bone. This didn't occur with the first method where the final bone had a very low thickness. In this method the comparisons between the original radiographic image and the generic model were all performed in the 2D space. Then the result of this comparison, that is the transform necessary to apply in the generic model, was applied to the 3D generic model in order to obtain the final bone model. The fact that these comparisons are performed in 2D space is an advantage relative to the first method. This is due to the fact that the computations in 2D are simpler than in 3D space. Also it makes unnecessary to perform triangulation of points, so it's not necessary to calibrate the system. Most of the times when a radiographic image is taken, the parameters of the system, that will be used on the calibration, are not appointed by the technician that performed the exam. So, this parameters are not known and need to be estimated. The estimation of the calibration introduces errors in the system which can lead to erroneous results as it was said in the previous section. So the fact that this isn't performed in this method eliminates one source of errors.

With this new method it was possible to obtain a 3D bone model aligned with the patient's radiographic image. Also, the scaling performed transformed the generic model so that it has the same size as the bone present in the radiographic image. All these transformations lead to a final

3D bone model aligned with the radiographic image and with the same size of the patient's bone. However, the shape of the bone is not the same as the patient's bone. This happens because there is one step that needs to be enhanced, that is the deformation step. This step was performed in 2D space as it was demonstrated. But, in 3D space it was not completed. It was tried to use the existing algorithms in ITK to perform deformation of meshes, however these algorithms were not successful. In these methods it's used a deformation field to deform the 3D model. When using a random deformation field, the final model appears to suffer only translation and not deformation. And when using the created deformation field, the initial and final model are the same. So the problem appears to be related with the algorithm of deformation and not with the creation of the deformation field. However it can also be errors in the creation of the deformation field, for example, the deformation field created had the same size, origin and direction as the radiographic image but it should be equal to the generic model. This is because the deformation field is an image of vectors where every pixel contains the deformation that will be applied in that pixel, so if the deformation field has the same size, origin and direction as the radiographic image it is not possible to know in each pixel of the model the deformation will be applied. So, these are the improvements that needs to be done in this method, with that finished it will be possible to obtain the final 3D bone model that corresponds to the patient's specific bone anatomy.

The previous work done related to this method had similar results to the ones achieved in this work [5, 8, 12, 38–40, 42–45, 47]. However, in their work they were able to perform deformation of the model, so that it has the same shape as the patient radiographic image. They performed this deformation using the computed 2D deformation field and the correspondences between the points of the model's projections and the 3D points of the generic model. With these correspondences it's possible know which point in the 3D model corresponds to the 2D point of the projection that suffered deformation and then apply the same deformation to the 3D point. In this work, these correspondences were not performed, instead a 3D deformation field was created from the 2D deformation field, by setting the z component of every vector to 0. So, with this deformation field, the model will be deformed in the plane xy, then it was intended to create another deformation field in the plane yz, using the lateral radiographic image. So, with this two deformation fields, the model will be deformed in the three directions (x,y,z). However, this second deformation field was not created because the application of the first deformation field was not successful as it was said before.

4.2 Conclusions

4.2.1 Description of the work

In the first chapter of this dissertation was presented an introduction about the importance of the surgery planning and the use of 3D bone models during that planning. It was also pointed the motivation that originate this work and the goals to achieve in its development. To finish the structure of the dissertation was described.

In the second chapter the medical imaging systems, referred throughout this work, were described. Also, in this chapter, the existing orthopedic surgery planning systems were analysed and the existing products in the market were pointed out. Still in this chapter previous works done to perform 3D reconstruction of bone structures from radiographic images are described. The existing methods are divided in two types.

The fourth chapter presents the methods developed in this work to achieve the 3D reconstruction from radiographic images. The data used and the results obtained are also presented.

The discussion of the results obtained is done in the fifth chapter. And some conclusions drawn from the developed work are highlighted.

4.2.2 Conclusions

In this work, it was developed a system to perform the 3D reconstruction of bone structures from radiographic images. In order to perform this reconstruction, two methods were developed. As it was seen in the previous chapter, the second method lead to better results than the first one. This was mainly due to the fact that the second method does not use triangulation of points and so it was not necessary to know the calibration parameters of the radiographic system. However, the second method needs to be improved. The last step of deformation was not achieved, possibly because the algorithm used was not working correctly. Investigating the causes of this problem and performing the deformation is the future work that needs to be done in order to complete this work. So, with this work, it was achieved a final 3D bone model aligned with the radiographic image and with the same size as the patient's bone. The only step that needs enhancement is the deformation that will make the final bone have the same shape as the patient's bone.

The system developed in this work can be integrated, in the future, in a commercial software that performs the pre-operative planning of orthopedic surgeries. This will be very helpful for the surgeons because they could evaluate the entire patient's bone anatomy, prepare for possible complications,

choose the most appropriate implant and all this with only radiographic images that have more advantages over the existing 3D direct imaging modalities (CT, MRI). The patient will also benefit from this system because the surgery accuracy will be enhanced and thus the risk of post-operative complications will decrease. The work developed here will have impact both in surgeons' and patients' life. The surgeon will be better prepared for the surgery, which will enhance its accuracy and reduce its time and the patients will have lower risk of suffering post-operative complications. This work can help improve the quality of life of the general population.

References

[1] P. Gamage, S. Q. Xie, P. Delmas, and W. L. Xu, ``Computer assisted 3D pre-operative planning tool for femur fracture orthopedic surgery,'' *Imaging*, vol. 7625, pp. 76 253D–76 253D–11, 2010.

[2] R. a. Robb, D. P. Hanson, and J. J. Camp, ``Computer-aided surgery planning and rehearsal at Mayo Clinic,'' *Computer*, vol. 29, no. 1, pp. 39–47, 1996.

[3] P. Gamage, S. Q. Xie, P. Delmas, and W. L. Xu, ``Diagnostic radiograph based 3D bone reconstruction framework: Application to the femur,'' *Computerized Medical Imaging and Graphics*, vol. 35, no. 6, pp. 427–437, Sep. 2011.

[4] N. Baka, B. L. Kaptein, M. de Bruijne, T. van Walsum, J. E. Giphart, W. J. Niessen, and B. P. F. Lelieveldt, ``2d-3d shape reconstruction of the distal femur from stereo x-ray imaging using statistical shape models.'' *Medical image analysis*, vol. 15, no. 6, pp. 840–50, Dec. 2011.

[5] M. Mahfouz, A. Badawi, E. E. A. Fatah, M. Kuhn, B. Merkl, K. Reconstruction, and B. X, ``Reconstruction of 3D Patient-Specific Bone Models From Biplanar X-Ray Images Utilizing Morphometric Measurements,'' in *Proceedings of the 2006 International Conference on Image Processing, Computer Vision, & Pattern Recognition, Las Vegas, Nevada, USA, June 26-29, 2006*, vol. 2, 2006.

[6] T. Cresson, R. Chav, D. Branchaud, L. Humbert, B. Godbout, B. Aubert, W. Skalli, and J. a. De Guise, ``Coupling 2D/3D registration method and statistical model to perform 3D reconstruction from partial x-rays images data,'' in *Proceedings of the 31st Annual International Conference of the IEEE Engineering in Medicine and Biology Society: Engineering the Future of Biomedicine, EMBC 2009*, 2009, pp. 1008–1011.

[7] W. Wei, G. Wang, and H. Chen, ``3D reconstruction of a femur shaft using a model and two 2D X-ray images,'' in *2009 4th International Conference on Computer Science & Education*. Ieee, Jul. 2009, pp. 720–722.

[8] H. Boussaid, E. C. Paris, and N. Paragios, ``3D Model-based Reconstruction of the Proximal Femur from Low-dose Biplanar X-Ray Images,'' pp. 1–10, 2011.

[9] J. Ribeiro and V. Alves, ``A Computed Tomography Based Orthopedic Surgery Planning solution,'' in *Computational Vision and Medical Image Processing IV: VIPIMAGE 2013*, Oct. 2013.

[10] J. Ribeiro, V. Alves, S. Silva, and J. Campos, ``A 3D Computed Tomography Based Tool for Orthopedic Surgery Planning,'' in *Developments in Medical Image Processing and Computational Vision*, 2014.

[11] C. Koehler, T. Wischgoll, and F. Golshani, ``Reconstructing the human ribcage in 3d with x-rays and geometric models,'' *IEEE Multimedia*, vol. 17, no. 3, pp. 46–53, 2010.

[12] S. Filippi, B. Motyl, and C. Bandera, ``Analysis of existing methods for 3D modelling of femurs starting from two orthogonal images and development of a script for a commercial software package,'' *Computer Methods and Programs in Biomedicine*, vol. 89, no. 1, pp. 76–82, Jan. 2008.

[13] ``Peekmed,'' http://www.peekmed.com, accessed: 2014-09-30.

[14] ``Itk - segmentation registration toolkit,'' http://www.itk.org, accessed: 2014-10-15.

[15] ``Vtk - the visualization toolkit,'' http://www.vtk.org, accessed: 2014-10-15.

[16] ``Overview of action research methodology,'' http://web.net/robrien/papers/arfinal.html#_Toc26184650, accessed: 2015-08-05.

[17] P. Suetens, *Fundamentals of Medical Imaging, Second Edition*, 2009.

[18] C. Guy and D. Ffytche, *An Introduction to The Principles of Medical Imaging*.

[19] J. Fessler, ``Physics of Projection Radiography,'' pp. 1–13, 2009.

[20] ``Medical x-ray imaging - computed tomography (ct),'' http://www.fda.gov/Radiation-EmittingProducts/RadiationEmittingProductsandProcedures/MedicalImaging/MedicalX-Rays/ucm115317.htm, accessed: 2014-11-30.

[21] ``Ct scan - mayo clinic,'' http://www.mayoclinic.org/tests-procedures/ct-scan/basics/definition/prc-20014610, accessed: 2014-11-30.

[22] D. J. Brenner and E. J. Hall, ``Computed tomography–an increasing source of radiation exposure.'' *The New England journal of medicine*, vol. 357, no. 22, pp. 2277–2284, 2007.

[23] R. Iorio, J. Siegel, L. M. Specht, J. F. Tilzey, A. Hartman, and W. L. Healy, ``A Comparison of Acetate vs Digital Templating for Preoperative Planning of Total Hip Arthroplasty. Is Digital Templating Accurate and Safe?'' *Journal of Arthroplasty*, vol. 24, no. 2, pp. 175–179, 2009.

[24] P. R. Krekel, P. R. Krekel, C. P. Botha, C. P. Botha, E. R. Valstar, E. R. Valstar, P. W. de Bruin, P. W. de Bruin, P. M. Rozing, P. M. Rozing, F. H. Post, and F. H. Post, ``Interactive simulation and comparative visualisation of the bone-determined range of motion of the human shoulder,'' *Proceedings of Simulation and Visualization*, pp. 275–288, 2006.

[25] ``Traumacad: Digital templating software for orthopedic surgeons,'' http://www.voyanthealth.com/traumacad.jsp, accessed: 2015-02-20.

[26] ``Orthoview orthopaedic templating digital pre-operative planning,'' http://www.orthoview.com/, accessed: 2015-02-20.

[27] ``Orthopedic templating software | orthocase | merge healthcare,'' http://www.merge.com/solutions/orthopedics/orthocase.aspx, accessed: 2015-02-20.

[28] ``Agfa healthcare - impax orthopaedic tools,'' http://www.agfahealthcare.com/brazil/pt/main/products_services/diagnostic_and_clinical_applications/diagnostic_clinical_applications/impax_orthopaedic_tools.jsp, accessed: 2015-02-20.

[29] N. Schep, I. Broeders, and C. van der Werken, ``Computer assisted orthopaedic and trauma surgery State of the art and future perspectives,'' *International Journal of the Care of the Injured*, vol. 34, pp. 299–306, 2003.

[30] ``Computer assisted surgery - knee navigation surgery: Stryker,'' http://biomedical.materialise.com/orthopaedic-engineering, accessed: 2014-12-10.

[31] R. Lattanzi, F. Baruffaldi, C. Zannoni, and M. Viceconti, ``Specialised CT scan protocols for 3-D pre-operative planning of total hip replacement,'' *Medical Engineering and Physics*, vol. 26, no. 3, pp. 237–245, 2004.

[32] L. Joskowicz, C. Milgrom, A. Simkin, D. Ph, L. Tockus, M. Sc, and Z. Yaniv, ``FRACAS : A System for Computer-Aided Image- Guided Long Bone Fracture Surgery image processing,'' *Computer Aided Surgery*, vol. 3, no. 6, pp. 271–288, 1998.

[33] ``Orthopaedic engineering | software services for biomedical engineering,'' http://www.stryker.com/en-us/products/Orthopaedics/ComputerAssistedSurgery/KneeNavigationSurgery/index.htm, accessed: 2014-12-10.

[34] R. Dumas, a. Le Bras, N. Champain, M. Savidan, D. Mitton, G. Kalifa, J. P. Steib, J. a. De Guise, and W. Skalli, ``Validation of the relative 3D orientation of vertebrae reconstructed by bi-planar radiography,'' *Medical Engineering and Physics*, vol. 26, no. 5, pp. 415–422, Jun. 2004.

[35] S. Kadoury, F. Cheriet, C. Laporte, and H. Labelle, ``A versatile 3D reconstruction system of the spine and pelvis for clinical assessment of spinal deformities.'' *Medical & biological engineering & computing*, vol. 45, no. 6, pp. 591–602, Jun. 2007.

[36] E. Jolivet, B. Sandoz, S. Laporte, D. Mitton, and W. Skalli, ``Fast 3D reconstruction of the rib cage from biplanar radiographs,'' *Medical and Biological Engineering and Computing*, vol. 48, no. 8, pp. 821–828, Aug. 2010.

[37] B. Zhang, S. Sun, J. Sun, Z. Chi, and C. Xi, ``3D Reconstruction Method from Biplanar Radiography Using DLT Algorithm: Application to the Femur,'' in *2010 First International Conference on Pervasive Computing, Signal Processing and Applications*. Ieee, Sep. 2010, pp. 251–254.

[38] S. Quijano, a. Serrurier, B. Aubert, S. Laporte, P. Thoreux, and W. Skalli, ``Three-dimensional reconstruction of the lower limb from biplanar calibrated radiographs,'' *Medical Engineering and Physics*, vol. 35, no. 12, pp. 1703–1712, Dec. 2013.

[39] P. Messmer, G. Long, N. Suhm, P. Regazzoni, and a. L. Jacob, ``Volumetric model determination of the tibia based on 2D radiographs using a 2D/3D database,'' *Computer Aided Surgery*, vol. 6, no. 4, pp. 183–194, Jan. 2001.

[40] K. Koh, Y. H. Kim, K. Kim, and W. M. Park, ``Reconstruction of patient-specific femurs using X-ray and sparse CT images.'' *Computers in biology and medicine*, vol. 41, no. 7, pp. 421–6, Jul. 2011.

[41] R. Donner, B. H. Menze, H. Bischof, and G. Langs, ``Global localization of 3D anatomical structures by pre-filtered Hough forests and discrete optimization.'' *Medical image analysis*, vol. 17, no. 8, pp. 1304–14, Dec. 2013.

[42] P. E. Galibarov, P. J. Prendergast, and a. B. Lennon, ``A method to reconstruct patient-specific proximal femur surface models from planar pre-operative radiographs,'' *Medical Engineering and Physics*, vol. 32, no. 10, pp. 1180–1188, Dec. 2010.

[43] Y. Chaibi, T. Cresson, B. Aubert, J. Hausselle, P. Neyret, O. Hauger, J. a. de Guise, and W. Skalli, ``Fast 3D reconstruction of the lower limb using a parametric model and statistical inferences and clinical measurements calculation from biplanar X-rays.'' *Computer methods in biomechanics and biomedical engineering*, vol. 15, no. 5, pp. 457–66, Jan. 2012.

[44] M. K. Lee, S. H. Lee, A. Kim, I. Youn, T. S. Lee, N. Hur, and K. Choi, ``The Study of Femoral 3D Reconstruction Process Based on Anatomical Parameters Using a Numerical Method,'' *Journal of Biomechanical Science and Engineering*, vol. 3, no. 3, pp. 443–451, 2008.

[45] X. Dong and G. Zheng, ``Automatic extraction of proximal femur contours from calibrated X-ray images using 3D statistical models : an in vitro study,'' *THE INTERNATIONAL JOURNAL OF MEDICAL ROBOTICS AND COMPUTER ASSISTED SURGERY*, vol. 5, no. April, pp. 213–222, 2009.

[46] S. Filippi, B. Motyl, and C. Bandera, ``Comparing parametric solid modelling/reconfiguration, global shape modelling and free-form deformation for the generation of 3D digital models of femurs from X-ray images,'' *Computer Methods in Biomechanics and Biomedical Engineering*, vol. 12, no. 1, pp. 101–108, Feb. 2009.

[47] M. Gunay, M.-B. Shim, and K. Shimada, ``Cost and time-effective three-dimensional bone-shape reconstruction from X-ray images,'' *THE INTERNATIONAL JOURNAL OF MEDICAL ROBOTICS AND COMPUTER ASSISTED SURGERY*, vol. 3, no. October 2007, pp. 323–335, 2008.

[48] ``Radiography (plain x-rays),'' https://www.medicalradiation.com/types-of-medical-imaging/imaging-using-x-rays/radiography-plain-x-rays/, accessed: 2014-11-30.

[49] ``Bel home page | biomed town portal,'' https://www.biomedtown.org/biomed_town/LHDL/Reception/datarepository/repositories/bel_home/, accessed: 2014-11-20.

[50] ``Multiplanar reconstruction (mpr),'' http://www.wikiradiography.net/page/Multiplanar+Reconstruction+(MPR), accessed: 2014-12-10.

[51] K. Rohr, H. S. Stiehl, R. Sprengel, T. M. Buzug, J. Weese, and M. H. Kuhn, ``Landmark-based elastic registration using approximating thin-plate splines,'' *IEEE Transactions on Medical Imaging*, vol. 20, no. 6, pp. 526–534, 2001.

[52] J. Canny, ``A computational approach to edge detection.'' *IEEE transactions on pattern analysis and machine intelligence*, vol. 8, no. 6, pp. 679–698, 1986.

[53] R. Hartley and A. Zisserman, *Multiple view geometry in computer vision*, 2004.

[54] A. Zisserman, D. Capel, A. Fitzgibbon, P. Kovesi, T. Werner, and Y. Wexler, ``Matlab functions for multiple view geometry,'' http://www.robots.ox.ac.uk/~vgg/hzbook/code/, accessed: 2015-04-30.

[55] R. Dumas, D. Mitton, S. Laporte, J. Dubousset, J. P. Steib, F. Lavaste, and W. Skalli, ``Explicit calibration method and specific device designed for stereoradiography,'' *Journal of Biomechanics*, vol. 36, no. 6, pp. 827–834, 2003.

[56] B. Zhang, J. Sun, Z. Chi, and S. Sun, ``3D Reconstruction of Patient-specific Femurs Using Coherent Point Drift,'' vol. 11, no. 2, pp. 1101–1110, 2013.

[57] B. Poling, ``A Tutorial On Camera Models,'' pp. 1–10.

[58] U. o. T. Jepson, Allan (Department of Computer Science, ``Camera Models,'' *Camera*, no. 1, pp. 32–44, 2005.

[59] G. Xu and Z. Zhang, *Epipolar Geometry in Stereo, Motion and Object Recognition*, 1996, vol. 6.

[60] F. Cheriet and J. Meunier, ``Self-calibration of a biplane X-ray imaging system for an optimal three dimensional reconstruction,'' *Computerized Medical Imaging and Graphics*, vol. 23, no. 3, pp. 133–141, 1999.

[61] S. Schumann, G. Zheng, and L.-P. Nolte, ``Calibration of X-ray radiographs and its feasible application for 2D/3D reconstruction of the proximal femur.'' *Conference proceedings : ... Annual International Conference of the IEEE Engineering in Medicine and Biology Society. IEEE Engineering in Medicine and Biology Society. Conference*, vol. 2008, pp. 470–473, 2008.

[62] S. Schumann, B. Thelen, S. Ballestra, L. P. Nolte, P. Büchler, and G. Zheng, ``X-ray image calibration and its application to clinical orthopedics,'' *Medical Engineering and Physics*, vol. 36, no. 7, pp. 968–974, 2014.

[63] D. C. Moura, J. G. Barbosa, A. M. Reis, and J. a. M. R. S. Tavares, ``A flexible approach for the calibration of biplanar radiography of the spine on conventional radiological systems,'' *CMES - Computer Modeling in Engineering and Sciences*, vol. 60, no. 2, pp. 115–137, 2010.

[64] S. Kadoury, F. Cheriet, and H. Labelle, ``Self-calibration of biplanar radiographic images through geometric spine shape descriptors,'' *IEEE Transactions on Biomedical Engineering*, vol. 57, no. 7, pp. 1663–1675, 2010.

[65] M. I. a. Lourakis, ``A Brief Description of the Levenberg-Marquardt Algorithm Implemened by levmar,'' *Matrix*, vol. 3, p. 2, 2005.

[66] H. P. Gavin, ``The Levenberg-Marquardt method for nonlinear least squares curve-fitting problems,'' *Department of Civil and Environmental Engineering, Duke University*, pp. 1–17, 2013.

[67] R. I. Hartley and P. Sturm, ``Triangulation,'' *Computer Vision and Image Understanding*, vol. 68, no. 2, pp. 146–157, 1997.

[68] ``Simple triangulation with opencv from hartley and zisserman,'' http://www.morethantechnical.com/2012/01/04/simple-triangulation-with-opencv-from-harley-zisserman-w-code/, accessed: 2015-03-10.

[69] M. Whitbeck and H. Guo, ``Multiple Landmark Warping Using Thin-Plate Splines,'' *Image Processing and Computer Vision*, no. 361, 2006.

[70] F. Bookstein, ``Principal Warps - Thin-Plate Splines and the Decomposition of Deformations,'' *IEEE Transactions on Pattern Analysis and Machine Intelligence*, 1989.

[71] A. Segal, D. Haehnel, and S. Thrun, ``Generalized-ICP,'' *Robotics: Science and Systems*, 2009.

Appendix A

Publications

A.1 3D Reconstruction of Bone Structures Based on Planar Radiography

Authors:

Ana Coelho, João Pedro Ribeiro, Jaime Campos, Sara Silva, Victor Alves

Conference:

ISAMI'15 - 6th International Symposium on Ambient Intelligence

Year:

2015

Abstract:

The 3D reconstruction of bone structures has many advantages in orthopedic applications. 3D bone models could be used in computer assisted surgery systems or in the pre-operative planning of an orthopedic surgery. The visualization of these models will lead to higher surgery accuracy. Usually the 3D reconstruction is done with CT or MRI scans. However these modalities have some disadvantages like the high costs, high acquisition time and high radiation. So, the planar radiography emerges as a more advantageous modality, because it avoids exposure to high radiation, reduces

the acquisition time and costs and also is the most usually acquired study in the pre-operative planning of an orthopedic surgery. The principal challenge in reconstructing bone models from planar radiography is that a lot of information is missing when only one or two orthogonal images are used. So it's hard to obtain a precise geometry of the bone structure with only this information. In this work, we present a solution for the problem of reconstructing bone structures from planar radiography. With this solution, it's possible to obtain a 3D model of the bone that is suitable for orthopedic surgery planning.

Keywords:

3D Reconstruction, Planar Radiography, Orthopedic Surgery Planning

State:

Published in http://link.springer.com/chapter/10.1007/978-3-319-19695-4_14

Glossary

DLT Direct Linear Transformation Algorithm is a technique used to find linear mappings between two data sets given a certain number of corresponding data points between the two data sets. It can be used in 3D reconstruction of points, in this case the mapping between 3D points in a scene and their projection onto the image plane is searched. It can also be used in camera calibration where once again the relation between 3D points and their corresponding 2D image points is searched. 14

FFD Free Form Deformation technique is employed in the deformation of rigid objects. It consists in embed a model in a cube or another hull object and by deforming the hull, the model will be deformed as well. 16

ICP Iterative Closest Point is an algorithm used to minimize the difference between two sets of points. Its main applications are the 2D or 3D reconstruction of surfaces from different scans, localization of robots and achievement of optimal path planning, to perform co-registration of models, etc. 42, 44, 45, 47, 48

IDE Integrated Development Environment is a programming environment that was packaged as an application program. Usually it consists in a code editor, a compiler, a debugger and a graphical user interface builder. It could be a standalone application or can be included as part of one or more existing and compatible applications. 4

MLS Moving Least Squares is a method used for smoothing and interpolating data. Shortly, is a method to reconstruct continuous functions from a set of unorganized points. This is done through the computation of a weighted least squares measure that is biased towards the region around the point being reconstructed. The method is used to reconstruct surfaces from sets of points. 16

MPR Multi Planar Reconstruction is a method to reconstruct volumes from CT scans. This method allows the reconstruction in different planes by cutting in slices the first volume reconstructed. With

this it's possible to have volumes in axial, coronal, sagittal and oblique planes. 21

NSCP Non Stereo Corresponding Points Algorithm is used to recover 3D coordinates of points that only appear in one image, unlike the points reconstructed with DLT that appear in at least two different images. In this case, it's known that the 3D position of the points will be in the line joining the x-ray source and the 2D point on the image. With this information, the 3D position of the points is found by deforming a generic object with geometrical and topological constraints. These constraints are defined accordingly to the structure that is being reconstructed. 14

PCA Principal Component Analysis is used in large datasets with the main goal of identify patterns. Through the analysis of the data, patterns will be found and this could help reduce the dimensions of the dataset with minimal loss of information. 15

SVD Single Value Decomposition corresponds to the factorization of a real or complex matrix. It is mainly used in signal processing and statistics applications. 36

TPS Thin Plate Splines is a spline-based technique employed for data interpolation and smoothing. It is a physical analogy that involves the bending of a thin sheet of metal. It can be used to compute the transformation over a set of points. 38